


PRIMER

A primer on stream temperature processes

Jason A. Leach¹  | Christa Kelleher² | Barret L. Kurylyk³ | R. Dan Moore⁴ | Bethany T. Neilson⁵

¹Natural Resources Canada, Canadian Forest Service, Great Lakes Forestry Centre, Sault Ste. Marie, Ontario, Canada

²Department of Civil and Environmental Engineering, Lafayette College, Easton, Pennsylvania, USA

³Department of Civil and Resource Engineering, Dalhousie University, Halifax, Nova Scotia, Canada

⁴Department of Geography, University of British Columbia, Vancouver, British Columbia, Canada

⁵Department of Civil and Environmental Engineering and Utah Water Research Laboratory, Utah State University, Logan, Utah, USA

Correspondence

Jason A. Leach, Natural Resources Canada, Canadian Forest Service, Great Lakes Forestry Centre, Sault Ste. Marie, Ontario, Canada.

Email: jason.leach@canada.ca

Funding information

Canadian Forest Service Sustainable Forest Management Program; Natural Sciences and Engineering Research Council of Canada, Grant/Award Number: RGPIN-2018-04637

Edited by: Jan Seibert and Wendy Jepson, Co-Editors-in-Chief

Abstract

Stream temperature is one of the most critical factors controlling aquatic ecosystem health. Practitioners and researchers from a range of fields, including biology, ecology, hydrology, engineering, and watershed management, are concerned with how climate and environmental changes are impacting stream thermal regimes. This primer provides an introduction to the various energy and water exchange processes that underpin stream temperature patterns from small headwater streams to large river systems. An overview of the various energy exchanges is provided, including (1) advection associated with hydrologic processes, and energy exchanges at (2) the stream–atmosphere interface and (3) stream–bed interface. The interaction and spatiotemporal variability of these energy exchange processes are discussed using a water and energy balance framework. A sound physical understanding and appreciation of the complex controls governing stream thermal regimes will help inform effective management strategies to sustain healthy aquatic ecosystems in a changing world.

This article is categorized under:

Science of Water > Science of Water

Science of Water > Hydrological Processes

Science of Water > Water Quality

Water and Life > Nature of Freshwater Ecosystems

KEYWORDS

advection, energy fluxes, hydrology, stream temperature, thermal regime

1 | INTRODUCTION

Water temperature is a key influence on stream systems since it controls a variety of biological, chemical, and physical processes, including nutrient cycling and fish distribution and survival (Armstrong et al., 2021; Demars et al., 2011; Jankowski & Schindler, 2019; Johnston et al., 2020; Webb et al., 2008). Built infrastructure, such as water treatment and power generation stations, can also be impacted by the temperature of water sourced from streams and rivers

This is an open access article under the terms of the [Creative Commons Attribution-NonCommercial License](https://creativecommons.org/licenses/by-nc/4.0/), which permits use, distribution and reproduction in any medium, provided the original work is properly cited and is not used for commercial purposes.

© 2023 His Majesty the King in Right of Canada and The Authors. *WIREs Water* published by Wiley Periodicals LLC. Reproduced with the permission of the Minister of Natural Resources Canada.

(Delpla et al., 2009; van Vliet et al., 2012). Stream thermal regimes naturally vary across spatiotemporal scales due to complex interactions between energy exchange and hydrologic processes (Fullerton et al., 2015; Kelleher et al., 2012; Poole & Berman, 2001; Steel et al., 2017), and can be altered by climate variability and land cover changes such as urbanization, wildfire, and forestry (Dunham et al., 2007; Moore, Spittlehouse et al., 2005; Nelson & Palmer, 2007). There is a critical need to understand and predict stream temperature dynamics and responses to environmental change in order to sustain healthy aquatic ecosystems (Caissie, 2006).

An understanding of stream temperature and its response to environmental change is relevant to a wide range of researchers and practitioners, including ecologists, hydrologists, engineers, and foresters, as well as fisheries, watershed and land managers. Many people interested in stream temperature may not have a technical background in thermodynamics or physical hydrology; therefore, the objective of this primer is to provide a primarily qualitative description of the various water and energy exchanges that control stream temperature. This discussion provides the conceptual framework for understanding how stream temperature varies over space (small headwater streams to large river systems) and time (daily, annual, and decadal scales). Existing reviews primarily focused on empirical syntheses, modeling approaches, or implications for aquatic ecosystems and provided only a cursory description of the physical energy exchange processes acting on streams (Caissie, 2006; Dugdale et al., 2017; Hannah & Garner, 2015; Ouellet et al., 2020; Poole & Berman, 2001; Webb et al., 2008); therefore, this primer fills a need by providing a detailed, but succinct, explanation of the stream energy balance framework. We mostly use examples of streams from mid-latitude forested environments in this primer; however, the conceptual approach outlined here can be broadly applied to streams in any geographical location.

2 | AN ENERGY AND WATER BALANCE PERSPECTIVE ON STREAM TEMPERATURE

Stream temperature variability is an expression of the energy and water cycling occurring in watersheds at and upstream of the point of measurement. For this reason, stream temperature has been used as an indicator of watershed runoff processes and groundwater–surface water interactions (Briggs et al., 2018; Shanley & Peters, 1988). Grounding our understanding of stream temperature patterns within a conceptual model that focuses on water and energy balances provides a rigorous approach for assessing and predicting stream temperature response to environmental change (Box 1).

BOX 1 Air and stream temperature correlations

In contrast to an energy-balance approach, correlations with air temperature are often used to investigate variability in stream temperature (Mohseni et al., 1998). This is partly due to air temperature being inexpensively and easily measured for many locations, compared to the extensive instrumentation and time needed to measure or estimate the various energy exchange processes controlling stream temperature (Figure 1). In addition, air temperature can be correlated with many of these energy exchange processes, such as incoming shortwave and longwave radiation, and sensible and latent heat fluxes, as well as heat inputs associated with precipitation that enters streams directly or indirectly as runoff from the land. Air temperature can therefore be a useful and effective proxy of these various energy fluxes and a first-order approach to help classify stream thermal regimes and their drivers (Hare et al., 2021; Isaak et al., 2017). However, care must be taken when assigning causality between air and stream temperature because the actual energy exchange processes controlling stream temperature are complex and not always directly influenced by air temperature. For example, air and stream temperatures may show high correlations because they are both responding to solar radiation (Johnson, 2003). In addition, multiple processes acting on the stream environment may be correlated with air temperature, and untangling their relative importance can be challenging. Under changing environmental conditions, the relationships between air temperature and the processes controlling stream temperature may not remain stable (Arisemendi et al., 2014; Leach & Moore, 2019). Therefore, grounding our understanding of stream temperature dynamics within a conceptual model that focuses on processes, and not just correlations, is the most rigorous approach for anticipating and assessing stream temperature response to environmental change.

Stream temperature is a measure of the heat content of the water flowing in the stream. This is analogous to how concentration of a solute is a measure of the amount of that solute in a volume of water. To understand how the energy and water balance influence stream temperature, it is important to understand the relationship between temperature, T ($^{\circ}\text{C}$), and heat, H (J):

$$T = \frac{H}{\rho C_p V} \quad (1)$$

where ρ is density (kg m^{-3}), C_p is specific heat ($\text{J kg}^{-1}\text{ }^{\circ}\text{C}^{-1}$), and V is volume (m^3) of water. Heat content is defined relative to a reference temperature or thermal datum (Saur & Anderson, 1956). In Equation (1), the reference temperature is implicitly defined as 0°C .

From Equation (1), we can see that if heat is gained or lost from a stream without water being added or removed (i.e., no change in volume), as is the case with radiation exchanges, for example, the stream temperature will change in direct proportion to the heat gained or lost:

$$\Delta T \propto \Delta H \quad (2)$$

During periods when the volume of water in a system is changing, such as occurs due to groundwater or tributary inflow to a stream reach, Equation (2) no longer holds. For example, addition of water that is at the same temperature as that already in the system will increase the heat storage, but will not change the temperature.

Since neither mass nor energy can be created or destroyed by ordinary means, an energy and water balance approach is a useful framework for considering how the fluxes in and out of a stream influence water temperature (Figure 1). An energy and water balance approach is universal in that these processes are acting on all streams in the world; however, stream temperature variability arises in time and space because the relative magnitudes and directions of these processes vary in time and space. Two general frameworks can be used for applying energy and water balances to stream systems: Lagrangian and Eulerian. These frameworks and their distinctions are outlined in Box 2. In this primer, we mostly use an Eulerian framework applied to different locations along a stream network (small headwater streams to large rivers) to discuss the relative importance of various energy exchanges through time.

3 | ENERGY EXCHANGE PROCESSES

The following sections outline the key energy exchanges in stream environments and how they vary across space, from headwater streams to large river systems (Figure 3), as well as at daily, annual, and decadal time scales. We lead with the advective fluxes since these set the stage for subsequent energy exchange processes and are not always fully recognized for their critical influence on stream temperature. We then address the energy fluxes at the water surface and stream-bed interfaces.

3.1 | Advection associated with hydrologic processes

3.1.1 | Advective fluxes

In the context of stream temperature, advection is the transfer of heat by movement of water; therefore, the water balance of a stream reach, and the heat transported by the water flowing in and out of a stream, is a fundamental control on stream temperature (Figure 1). Water can enter a stream reach by a variety of hydrologic pathways including tributaries, overland flow, shallow (e.g., <5 m beneath land surface, Hare et al., 2021) or deep subsurface flow, channel-intercepted precipitation, condensation, and inflows associated with stormwater and sewer systems, agricultural drainage networks or industrial effluent. Water can also leave a stream reach through losses to the subsurface by infiltration through the streambed and banks, evaporation, and water withdrawals for irrigation, industry, and other human uses. In all cases, these water inflows and outflows are associated with advective exchanges and have the potential to alter stream temperature directly by adding and removing heat, as well as indirectly by changing the width, depth, and velocity of water in the stream reach. In addition, changes to stream temperature due to advective exchanges will further

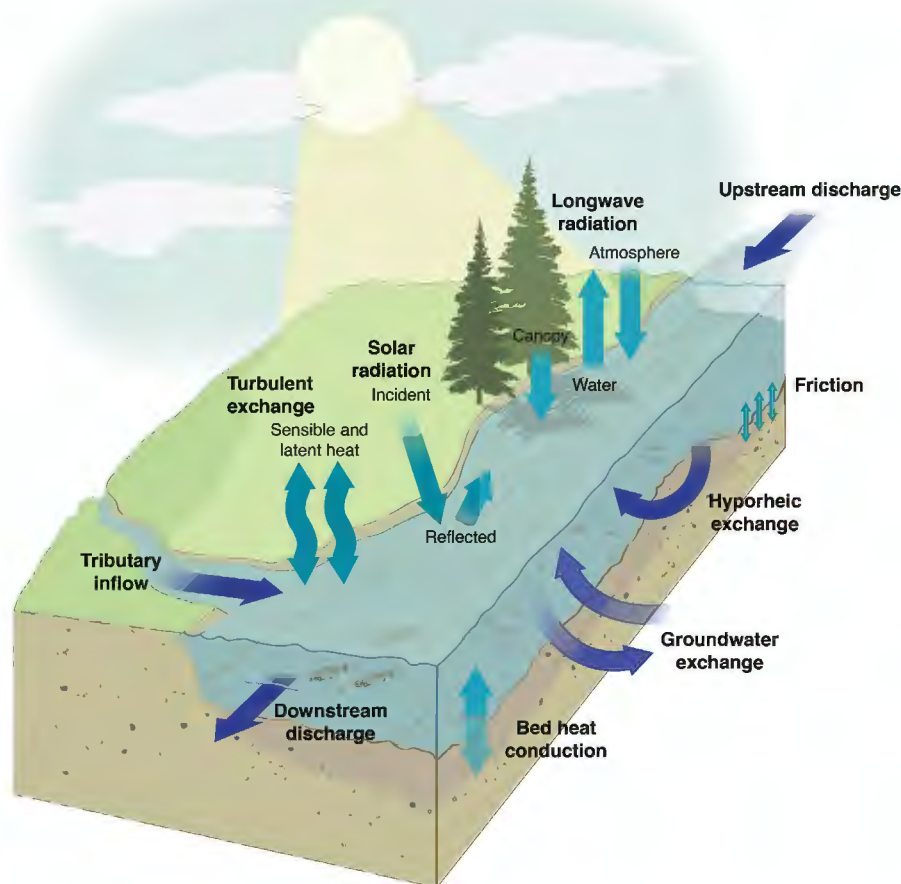


FIGURE 1 Diagram showing the various energy exchange processes acting on a stream reach. Surface energy fluxes include solar and longwave radiation, and sensible and latent heat. Energy exchanges at the streambed include bed heat conduction, hyporheic exchange, and friction. The advective fluxes associated with hydrologic processes (indicated by dark blue arrows) include surface inflows from tributaries and subsurface inflows and outflows from groundwater and hyporheic exchanges. In addition, in-stream flow (upstream and downstream discharge) can add and remove heat from the stream section of interest.

alter other energy exchanges that are a function of water temperature, such as outgoing longwave radiation, bed heat conduction, and the sensible and latent heat fluxes.

In addition to lateral inflows to and outflows from the stream, longitudinal advection within the stream network (i.e., heat transported in the downstream direction by in-stream flow) can also be an important energy flux. When applying an Eulerian framework (Box 2), longitudinal advection can occur due to water entering the stream segment of interest at the upstream boundary and leaving the stream segment at the downstream boundary. The importance of longitudinal advection will be proportional to the longitudinal temperature gradient (i.e., the rate at which temperature changes with downstream distance at a given time, Moore & Leach, 2021). High thermal gradient conditions tend to occur where there are significant and abrupt longitudinal changes in surface energy exchanges and discharge—for example, where riparian vegetation structure changes rapidly, such as downstream of a clearcut-forest transition (Moore, Sutherland, et al., 2005), or downstream of a tributary.

Heat within a stream can be transported longitudinally by dispersion in addition to advection. Whereas advection refers to the transport associated with the mean velocity of flow, dispersion results from variations in velocity with depth and across the channel due to the frictional effects of the bed, banks, and morphological features such as riffles, pools, and large wood pieces. Dispersion may be important for complex headwater streams in which transient storage processes (e.g., low water velocity features such as pools and backwater areas) have a significant influence on longitudinal transport. For larger streams that are less influenced by transient storage within the channel, the influence of

BOX 2 Bridge versus boat: Eulerian and Lagrangian frameworks for describing stream energy balances

Energy and water balance frameworks can be applied to stream systems using two distinct frames of reference (Figure 2). First, we could observe the stream from a bridge or a location along the bank and consider how temperature responds to water and energy exchanges through time for that fixed point or segment along a stream (Sinokrot & Stefan, 1993; Sridhar et al., 2004). This so-called Eulerian approach is typical of how most stream observations are collected (i.e., sensors installed at fixed locations within stream networks). In contrast, we can follow a parcel of water as it flows down a stream network and track all the water and energy inputs and outputs to and from the parcel (Gu et al., 1998; Vugts, 1974). This is called a Lagrangian approach and is conceptually similar to being in a boat and observing how the stream conditions change as the boat floats downstream. In reality, water does not move as a single parcel downstream. Instead, individual water molecules have varying velocities and flowpaths that result in a distribution of downstream travel times. This phenomenon is known as longitudinal dispersion and can be thought of as many small boats floating down a stream at different velocities. Accounting for dispersion within an Eulerian framework is relatively straightforward. Lagrangian stream temperature models do not account for dispersion, which may not introduce significant error for systems where longitudinal advection dominates (Leach & Moore, 2011; Sinokrot & Stefan, 1993).

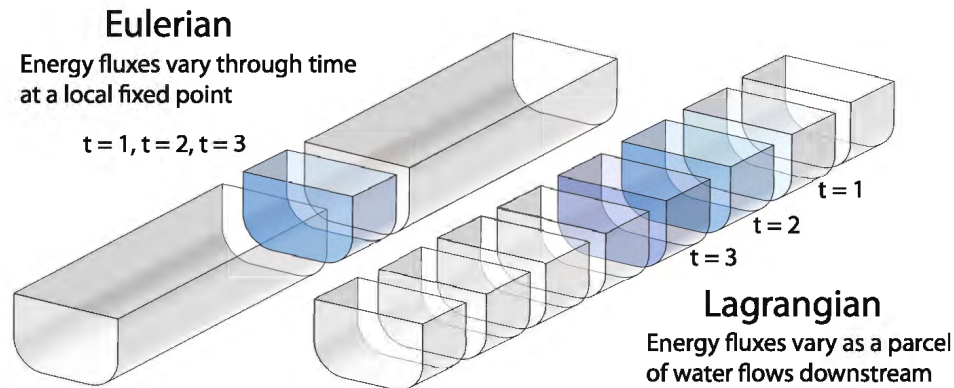


FIGURE 2 Graphical comparison of Eulerian and Lagrangian stream energy balance frameworks. An Eulerian framework considers how energy fluxes vary through time (t) at a fixed point, whereas a Lagrangian framework considers how energy fluxes vary for a water parcel as it flows downstream.

dispersion on heat transport can often be ignored (Sinokrot & Stefan, 1993). Whether longitudinal dispersion is relatively important or not for a given stream has implications for how these systems are modeled (Box 2).

When accounting for advective exchanges and their influence on stream temperature, it is important to consider both the discharge (i.e., volumetric flow rate, m^3s^{-1}) and temperature of water inflows and outflows of a stream reach. A small inflow discharge relative to the stream discharge, such as a small headwater stream draining into a large river, will have minimal impact on the average temperature of the receiving water body. In contrast, a large inflow discharge relative to the stream discharge can substantially alter stream temperature, but only if the temperature of the inflow is different from that of the receiving stream (Briggs & Hare, 2018; Leach et al., 2017). While advection associated with water inflows will always increase the amount of heat stored in a stream reach (assuming a thermal datum of 0°C), stream temperature can decrease, increase or not change depending on the temperature difference between the inflow source and the receiving stream (Kurylyk et al., 2016). In contrast, water losses from the stream will not directly alter stream temperature despite the removal of heat as long as the stream water is well mixed, since mass and heat are being removed proportionally.

In addition to directly adding or removing heat, water inflows, and outflows also indirectly impact stream thermal dynamics by altering the volume-to-surface area ratio and velocity of water in the stream channel (Gu et al., 1998;

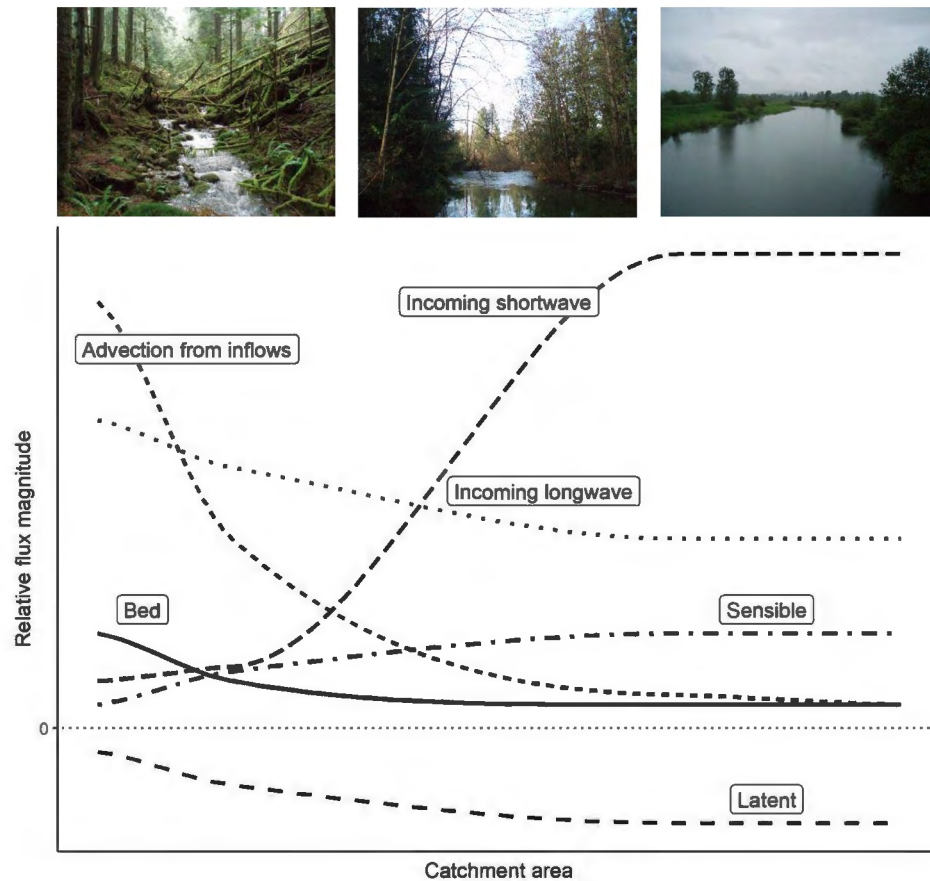


FIGURE 3 Conceptual relationships between stream size (as indicated by catchment area) and relative flux magnitudes. The relative flux magnitudes are mean seasonal values for a summer period (i.e., diel variations are averaged). Energy into the stream is represented as positive values, and energy away from the stream is represented by negative values. Images at the top provide visual examples of corresponding stream sizes. Advection from inflows refers to the heat flux associated with water inflows to the stream from surface and subsurface flow pathways.

Schmadel et al., 2015). This is important because the volume-to-surface area ratio of a stream channel, which can be mathematically simplified to the mean stream depth, influences how stream temperature responds to energy fluxes, such as solar radiation. The temperature of shallow streams will be more responsive to surface energy fluxes than the temperature of deep streams (Arscott et al., 2001; Mihalevich et al., 2020). In addition, stream velocity is also a function of in-channel water storage for a given location along a stream, and this has implications for stream temperature. From a Lagrangian perspective, water parcels in high-velocity streams will spend less time exposed to local energy exchange conditions than those in low-velocity streams (Garner et al., 2014). For example, a stream flowing through a section with high solar radiation inputs, such as a localized clearing, will experience less warming if water velocities are high compared to low velocities. In addition, structures such as beaver dams and resulting ponds within the stream network can strongly influence water velocities, which can result in spatial variability in stream temperature (Majerova et al., 2020).

3.1.2 | Variability in space and time

The magnitude of advective fluxes and how they vary in space and time are clearly tied to the hydrologic regime. The temperature and discharge of inflows will depend on the water source (e.g., rain, snowmelt, glacier melt, or human-related sources such as agricultural runoff, industrial effluent, and urban stormwater) and flow pathways, such as water entering a stream from overland, shallow subsurface or deep groundwater flow. For example, snowmelt water will enter the stream primarily during spring or mid-winter melt events and be close to 0°C, although the temperature may

increase as the melt water flows through the subsurface before reaching the stream (Kobayashi, 1985; Kurylyk et al., 2015; Leach & Moore, 2014; St-Hilaire et al., 2000). In contrast, the timing of industrial effluent to a stream may depend on operational schedules, and the temperature of these inflows may be relatively stable throughout the year (Schliemann et al., 2021; Xin & Kinouchi, 2013). The magnitude and timing of advective energy exchange will vary with factors that control hydrologic regimes, such as climate, topography, soil, land cover, and geology, as well as infrastructure, such as dams, reservoirs, and irrigation networks (Devito et al., 2005).

Except perhaps for rivers with significant tributaries, advection associated with surface and subsurface inflows is generally most important for smaller streams. This is because the ratios of inflow discharge to stream discharge are greater than for larger streams; therefore, the importance of advective inflows generally declines further down the stream network (Figure 3). Even when the inflow magnitude from subsurface flow or tributaries is small relative to stream discharge, these inflows can create localized temperature anomalies that can provide important thermal refuges for aquatic organisms such as fish (Dugdale et al., 2019; Ebersole et al., 2001; Torgersen et al., 1999).

In addition to lateral inflows, water exchanges at the stream surface by precipitation, condensation, and evaporation also contribute to advective heat transfer. Advection associated with direct precipitation interception by the channel is typically too small to influence stream temperature; however, snowfall onto the water surface, and the resulting consumption of heat from the streamwater to melt the snow, can result in abrupt drops in temperature for small streams during low flows (Leach & Moore, 2017; Roesky & Hayashi, 2022). Condensation and evaporation are also associated with advection due to the sensible heat of the water added or gained during vapor transfer at the surface, in addition to the latent heat transfer. The advective heat transfer associated with condensation and evaporation has been found negligible in lake heat budget studies (e.g., Richards et al., 2012; Sturrock et al., 1992) and is generally ignored in stream heat budget modeling (Neilson, Chapra, et al., 2010; Sinokrot & Stefan, 1993).

Lakes and reservoirs are common features in many stream networks and have the potential to influence downstream thermal regimes (Jones, 2010; Maheu et al., 2016; Verpoorter et al., 2014). Lakes and reservoirs can exhibit thermal regimes that differ from those of streams because they are typically less shaded than streams with riparian vegetation, can develop thermal stratification with outlet temperatures elevated relative to typical stream temperatures, and sometimes exhibit seiche (i.e., oscillating water levels associated with standing waves within the lake), which can result in sub-diel variations in outlet temperature (Lisi et al., 2015; West & Moore, 2020). These characteristics can generate strong longitudinal temperature gradients and thus longitudinal advective fluxes in downstream reaches (Leach et al., 2021). Lakes and reservoirs can also control downstream flow by moderating peakflows and augmenting low flows in the case of natural lakes, and through operational flow releases in the case of dams and reservoirs (Hayes et al., 2017). Together, these processes can influence downstream thermal regimes for distances up to tens of km or more (Dibble et al., 2021; Heavilin & Neilson, 2012; Olden & Naiman, 2010; Risley et al., 2010; Troxler & Thackston, 1977).

Variability in advective fluxes through time is also connected to the hydrologic regime. Inflows due to rainfall, snowmelt, and glacial meltwater can be important energy inputs at event and seasonal scales (Brown & Hannah, 2007, 2008). In contrast, groundwater inflows are more stable through time, both in terms of magnitude and temperature (Kurylyk, MacQuarrie, et al., 2014). Due to this stability, groundwater can have an important moderating influence on stream thermal regimes by elevating stream temperature in the winter and depressing stream temperature in the summer (Constantz, 1998). Although groundwater magnitude and temperature can be relatively stable at diel and annual time scales, they vary at decadal scales in response to changes in land surface temperature and groundwater recharge timing and rates (Kurylyk, MacQuarrie, & McKenzie, 2014; Menberg et al., 2014). Finally, advective fluxes associated with human infrastructure, such as reservoir releases or effluent discharge, will primarily depend on operation schedules and climate, as is the case of water release timing and depth of intake pipes for reservoirs that undergo seasonal thermal stratification (West & Moore, 2020).

3.2 | Stream surface exchanges

3.2.1 | Solar radiation

All bodies that have a temperature above absolute zero emit radiation, but the wavelength varies depending in part on the emitting body's temperature. The sun and earth have different surface temperatures (~6000 K vs. ~300 K), which generate radiation spectra that have limited overlap. Accordingly, we can classify radiation from the sun as solar or

shortwave radiation (with wavelengths in the 0.15–3 μm range) and radiation from the earth system, such as the atmosphere, water, terrain, vegetation, and buildings, as longwave radiation (wavelengths in the 3–100 μm range).

Solar radiation, often a dominant source of energy to streams (Webb & Zhang, 1999), reaches the stream surface as both direct and diffuse radiation (Moore, Spittlehouse, et al., 2005). Direct, or direct beam, radiation is that portion of radiation from the sun that is not absorbed or scattered as it travels through the atmosphere (Figure 1). Diffuse radiation is the portion of solar radiation that is reflected and scattered in the atmosphere by clouds and other aerosols. Direct solar radiation arrives at the stream surface as a function of the sun's position in the sky, and can be fully or partially blocked by surrounding terrain or vegetation. In contrast, diffuse radiation can arrive at the stream surface from all parts of the sky area as long as vegetation, terrain, or other features do not block the path. The fraction of diffuse radiation that reaches the stream surface is a function of the distributions of diffuse radiation and shade elements across the sky dome (Mihalevich et al., 2020). Diffuse radiation is commonly assumed to be isotropic (i.e., diffuse radiation arrives equally from all parts of the sky dome for a given time). Under this assumption, the fraction of diffuse radiation that reaches a given location on the surface is given by the location's sky view factor. While the sky view factor is often described as the ratio of open sky area to total area (open sky, vegetation, and terrain) that is "seen" by a point on the surface, its formal definition is more complicated and involves integrating a trigonometric function of the zenith angle over the gap areas (Moore, Sutherland, et al., 2005; Oke, 1987). Total incoming solar radiation can be primarily composed of diffuse radiation during twilight (i.e., when some solar radiation is received at a stream surface during dawn and dusk while the sun is still below the horizon) or during periods of extensive cloud cover.

A proportion of the solar radiation arriving at the stream surface is reflected; the ratio of reflected to absorbed radiation is referred to as the surface albedo. The albedo of water varies and is typically between 0.03 and 0.10 (King & Neilson, 2019; Leach & Moore, 2010), but can be higher if the water is aerated, has high turbidity, or if the sun is at a low angle in the sky (Neilson, Hatch, et al., 2010; Richards & Moore, 2011). Surface albedo also depends on the relative fractions of direct and diffuse radiation as well as surface roughness (McMahon & Moore, 2017). The fraction of radiation that is not reflected penetrates the water column and is typically absorbed by the water and streambed (Evans et al., 1998; Neilson et al., 2009). In some cases, where the stream is shallow and clear with light-colored bed material, a portion of incoming solar radiation can be reflected from the bed and ultimately leave the stream (Bray et al., 2017); therefore, measured stream albedo can be an aggregate of both the surface water and streambed albedos. Radiation that is absorbed at the streambed is transferred downwards by conduction (and by advection where water is infiltrating the bed) and upwards to the water column by conductive heat transfer in the laminar boundary of the bed (typically on the order of mm or lower thickness) and by turbulent transfer in the overlying water (Moore, Spittlehouse, et al., 2005). Except in pools and other slow-flowing zones, turbulent transfer dominates and provides efficient transport of heat from the bed to the water column.

Riparian vegetation and topography, such as incised valleys or steep channel banks, can block incoming solar radiation (Rutherford et al., 1997), especially for headwater streams in temperate mid-latitude environments due to the combination of narrow channel widths and the presence of riparian forest (Benyahya et al., 2012; MacDonald et al., 2014; Moore, Sutherland, et al., 2005). However, in cases where there is no riparian vegetation or it has been removed due to harvesting, wildfire, or urbanization, the temperature of small streams can be elevated due to incoming solar radiation since the mean water depths in these systems are relatively low (Brown & Krygier, 1970; Hannah et al., 2008).

As channel width increases as one moves from headwater streams to larger streams and rivers, the amount of solar radiation reaching the water surface increases since more stream surface area is exposed and is not effectively shaded by riparian vegetation or topography (Hebert et al., 2011). Variability in incident solar radiation at these scales becomes partly dependent on channel orientation, as streams oriented north–south may receive high incoming solar radiation during midday, whereas streams oriented west–east may be effectively shaded by riparian vegetation located on the equatorial-facing bank. For large and wide rivers, there is little potential for vegetation or topography to shade the stream. Exceptions are heavily incised channels where canyon-type structures can provide substantial shade even for large rivers, such as sections of the Colorado River that flow through the Grand Canyon (Mihalevich et al., 2020).

Incoming solar radiation varies at both diel and annual time scales. Solar radiation peaks during local noon and is zero during night when the sun is sufficiently below the horizon so that diffuse radiation no longer arrives at a surface. At annual time scales, solar radiation peaks at summer solstice and is lowest during winter solstice. Weather conditions cause solar radiation to vary at short to medium time scales (minutes to weeks), primarily as the result of changes in cloud cover. Other seasonal factors, such as smoke from wildfire, can periodically reduce incoming solar radiation (David et al., 2018). At decadal scales, solar cycles and global aerosol contents can modulate incoming solar radiation (Sanroma et al., 2010; Wild et al., 2005).

3.2.2 | Longwave radiation

Net longwave radiation exchange at the stream surface is the balance between incoming longwave radiation from the atmosphere, terrain, and vegetation canopy, and the outgoing radiation from the stream surface (Figure 1). The Stefan–Boltzmann law states that the radiative energy emitted by a surface is proportional to the fourth power of its absolute temperature as well as the surface emissivity, which is a measure of the efficiency at which the surface radiates relative to a theoretical black body. Generally, most natural surfaces, such as terrain, forests, and water, have relatively high emissivities, typically 0.95–0.98 (Oke, 1987), whereas atmospheric emissivity is often lower, except during cloudy or smoky conditions (Aubry-Wake et al., 2022). Similar to diffuse solar radiation, incoming longwave radiation is generally assumed to arrive equally from all parts of the sky area; therefore, the relative fractions of open sky, terrain, and forest canopy (i.e., view factors) that a stream “sees” control the amount of incoming longwave radiation that reaches the stream surface. Longwave radiation is nearly completely absorbed at the stream surface and only a small amount, typically about 3%, is reflected or transmitted into the water column (Anderson, 1954; Kirk, 2011).

Differences in emissivity between the sky and terrain/vegetation are the primary drivers of spatial variability in incoming longwave radiation along stream networks (Benyahya et al., 2012). Headwater streams typically receive greater amounts of incoming longwave radiation than larger streams due to the greater proportion of the stream’s view factor being composed of vegetation and terrain, which typically have higher emissivities than the atmosphere (Benyahya et al., 2012), as well as higher surface temperatures than the atmosphere during daytime (Cardenas et al., 2014). In addition, headwater streams are generally cooler than higher-order streams during summer (Fullerton et al., 2015; Wehrly et al., 2006); therefore, the outgoing longwave radiation flux is lower for headwater streams than larger streams.

Temporal variability in incoming longwave radiation is partly driven by temperatures of the atmosphere, terrain, and vegetation in the stream’s sky view, which generally peak during afternoon at daily scales and in summer at seasonal scales (Klos & Link, 2018). Weather systems and their influence on cloud cover result in increased incoming longwave radiation to the stream surface. At decadal scales, increases in air temperature and atmospheric water vapor content associated with climate change should result in overall increases in longwave radiation emitted from the atmosphere (Held & Soden, 2000; Luce et al., 2014). Due to the high heat capacity of water, which reduces diel and seasonal stream temperature variability, outgoing longwave radiation tends to be more stable through time.

3.2.3 | Sensible and latent heat

In addition to radiative exchanges at the stream surface, energy is also exchanged with the atmosphere as sensible and latent heat. Sensible heat exchange is the transfer of energy driven by temperature differences between the stream surface and the air mass directly above the stream; the heat transfer is from areas of higher temperature to areas of lower temperature. The sensible heat flux is so named because the transfer of energy can be sensed as a change in temperature. In contrast, latent heat exchange is associated with the phase change that accompanies evaporation or condensation at the stream surface. Evaporation represents a loss of heat and mass from the water column, and occurs when the air near the water surface has a higher vapor density than the ambient atmosphere, producing upward transport of water vapor. Condensation represents a gain of heat and mass, and occurs when the ambient atmosphere has a higher vapor density than the air near the water surface.

The exchange mechanisms for sensible and latent heat differ between the laminar and turbulent boundary layers. The laminar boundary layer extends from the water surface to a height of typically less than a few mm, with airflow parallel to the stream surface (Oke, 1987, fig. 2.3). Heat transfer in the laminar boundary layer occurs by conduction (sensible heat) and molecular diffusion (latent heat), which are relatively slow processes. The turbulent boundary layer lies above the laminar boundary layer, and is characterized by air flow that includes vertical eddies, which transport heat and mass between the surface and overlying air. Transfers of heat and water vapor within the turbulent boundary layer, often called convection, are more efficient than conduction and diffusion.

High wind speeds will typically generate greater heat and water vapor exchange by reducing the thickness of the laminar boundary layer and increasing turbulence, provided there are also temperature and humidity gradients between the stream surface and overlying air mass. Vertical convective mixing in the turbulent boundary layer also depends on atmospheric stability, which is a function of wind speed and the temperature difference between the surface and the ambient atmosphere. Where the water surface is warmer than the overlying air, the atmosphere will be

unstable because the less-dense air near the surface will experience an upwards buoyant force, which enhances vertical exchange. On the other hand, stable conditions occur when the surface is cooler than the overlying air, and density gradients suppress vertical motion (Oke, 1987).

Spatiotemporal variability in the direction and magnitude of the turbulent energy fluxes is a function of above-stream microclimate conditions, and temperature and humidity gradients between the stream surface and overlying air. For many streams during warmer seasons, the water column is typically cooler than the air during daytime and warmer during nighttime, resulting in the sensible heat flux adding energy to the stream during day and removing energy during night. Similar patterns emerge at seasonal scales, as streams can be warmer than air during winter, especially when influenced by groundwater discharge, and cooler than air during summer (Hannah et al., 2008; Leach & Moore, 2010).

Headwater streams tend to experience low wind speeds due to the sheltering effects of riparian vegetation and stream banks (Benyahya et al., 2010; Guenther et al., 2012; Gulliver & Stefan, 1986); therefore, these fluxes are usually minor energy balance terms since the turbulent exchange is limited under these conditions (Brown, 1969; Garner et al., 2015; Story et al., 2003). The magnitudes of the turbulent fluxes can also be suppressed on warm summer days by stable atmospheric conditions associated with the water surface typically being cooler than the ambient air (Caissie, 2016). The sensible and latent heat fluxes are generally greater for larger streams and rivers that are more exposed to wind (Benner, 2000; Maheu et al., 2014).

In addition to larger rivers having generally higher wind speeds than small sheltered streams, larger rivers also tend to have higher water temperatures during summer periods, which further contributes to latent heat exchange. The air immediately adjacent to the water surface will have a vapor density (the mass of water vapor per unit volume of air) equal to the saturation value associated with the water temperature. Because saturation vapor density has an approximately exponential relation with water temperature, increasing water temperature is usually associated with an increase in vapor density gradients that drive evaporation and thus latent heat loss. Hence, the latent heat flux can be an important mechanism for limiting stream warming during summer periods when incoming solar radiation is high, especially for larger streams that experience higher wind speeds (Benner, 2000; Caissie et al., 2007).

Above-stream microclimate conditions and stream-atmosphere humidity gradients tend to favor evaporation over condensation in most regions (Hannah et al., 2008; Leach & Moore, 2010; Webb & Zhang, 1999); however, condensation at the stream surface can happen when vapor density at the stream surface is lower than in the air mass above the stream. These conditions occur when the air above the stream has high humidity, such as during rainfall events (Caissie, 2016). Story et al. (2003) hypothesized that transpiration from overhanging vegetation in a poorly ventilated headwater stream environment was the cause of vapor density gradients conducive to condensation on the stream surface.

3.3 | Streambed exchanges

Energy exchanges at the streambed occur as conduction, advection (including hyporheic flow), and heat generated by friction (Figure 1). In addition, solar radiation can penetrate the water column and be absorbed or reflected at the streambed, as discussed previously.

3.3.1 | Bed conduction

Heat conduction occurs through the transfer of energy between adjacent molecules in response to a temperature gradient. All substances with an absolute temperature greater than 0 K manifest thermal energy as molecular-scale oscillations, the kinetic energy of which is related to temperature. Where a temperature gradient exists, this kinetic energy will be transferred from higher-energy molecules to adjacent lower-energy molecules, effectively transferring heat from warmer areas to cooler areas. The rate of heat conduction is proportional to the temperature gradient; the constant of proportionality is the thermal conductivity. In a streambed, the thermal conductivity varies due to the material composition and structure of the bed, degree of saturation, and the temperature of the sediment. Generally, saturated beds dominated by coarse grains, such as gravel and cobble, have higher thermal conductivities than beds dominated by fine grains, such as clay and silt, due primarily to differences in bulk density and mineralogy (Lapham, 1989). Due to the efficiency of heat transfer between the bed surface and the turbulent flow of water over the bed, the bed temperature at its surface is typically similar to the stream temperature (Sinokrot & Stefan, 1993); however, this is not always the case in areas with upwelling groundwater or in

shallow slow-moving areas where substantial solar penetration warms the sediments (Caissie et al., 2014; Neilson, Chapra, et al., 2010). The bed temperature below the bed surface will be influenced by conduction within the bed and advective fluxes associated with groundwater and hyporheic flow. For example, groundwater downwelling promotes lower vertical thermal gradients and conduction at the streambed interface, while groundwater upwelling results in higher vertical thermal gradients and streambed conduction (Caissie & Luce, 2017).

Bed conduction is a less efficient energy exchange than those at the stream surface and advective fluxes; therefore, the importance of bed conduction relative to other fluxes acting on a stream is greatest for headwater streams because other fluxes can be minimal due to shade and sheltering by riparian vegetation (Johnson, 2004). In addition, for streams that experience seasonal ice and snow cover, and a corresponding reduction in energy exchanges at the stream surface, bed conduction can be an important influence on stream temperature (Caissie et al., 2014; Kobayashi et al., 1994; Wankiewicz, 1984). Bed conduction becomes quickly overwhelmed by other fluxes further downstream in larger-order rivers (Hebert et al., 2011). Bed conduction primarily acts to damp diel fluctuations in stream temperature by being a heat loss during day and a heat source during night (Moore, Sutherland, et al., 2005). Similarly, at seasonal scales, heat flow is generally into the bed during summer and away from the bed to the stream during winter (Hannah et al., 2008).

3.3.2 | Hyporheic exchange

Hyporheic heat exchange is an advective flux associated with a two-way transfer of water and heat between the stream and the sediments of the bed, banks, and riparian zone (Findlay, 1995; Wondzell, 2011). Hyporheic water exchange typically occurs at changes in channel gradient, such as at sand ripples, riffle- and step-pool units, and large in-stream wood features, or where water is able to flow laterally through the bank at stream meanders (Boano et al., 2014; Tonina & Buffington, 2009). Hyporheic exchange is usually distinguished from groundwater in that the water originates as stream water, flows through the bed or bank, and returns to the stream some distance downstream. Since groundwater can be recharged by surface water, such as streams, wetlands, and lakes, in addition to precipitation-sourced recharge, the distinction between hyporheic and groundwater flow can be fuzzy and depends on the scale of investigation (Boano et al., 2014).

Hyporheic exchange is often conceptualized as not altering the stream water budget, since hyporheic losses and gains are assumed to be balanced at reach scales (Neilson, Chapra, et al., 2010). Therefore, hyporheic exchange impacts stream temperature only when the temperature of hyporheic water re-entering the stream is different from that of the stream water (Leach & Moore, 2014). These differences can arise as water flowing through the hyporheic zone is modified by energy exchanges within the bed and mixing with groundwater, as well as the effect of different hyporheic flowpath lengths desynchronizing hyporheic return flow temperatures from stream temperatures (Arrigoni et al., 2008). Since hyporheic exchange can also influence streambed temperatures, complex interactions arise between hyporheic exchange and bed conduction, as well as upwelling groundwater (Arrigoni et al., 2008; Guenther et al., 2014; Moore, Sutherland, et al., 2005). These interactions generate complex energy dynamics within the streambed that are challenging to observe and model (Caissie & Luce, 2017).

Hyporheic heat exchange is typically more important in smaller streams than larger streams, but also depends on stream discharge (Wondzell, 2011). Headwater streams tend to have steeper channel gradients and more complex morphologies, such as step-pool units, which are more conducive to hyporheic exchange than morphologies typically found in larger streams (Cardenas, 2015; Ward, 2016). Smaller streams also tend to experience greater diel fluctuations in stream temperature than larger streams, which result in greater potential for temperature differences between stream water and discharging hyporheic water. In addition, the proportion of stream water flowing through the hyporheic zone is typically greater for small streams than large streams; therefore, the returning hyporheic flow has a greater potential to influence stream temperature. While hyporheic heat exchange is typically a less important term in the overall energy balance of large streams compared to small streams, localized temperature anomalies created by hyporheic exchange in larger river systems can still provide important thermal environments for aquatic organisms (Arrigoni et al., 2008).

Similar to bed conduction, hyporheic exchange typically acts to moderate diel stream temperature patterns by acting as a heat loss during day and a heat source during night for summer periods (King & Neilson, 2019). The magnitude and direction of the hyporheic heat flux will vary at seasonal and annual scales in response to variations in stream discharge and stream and bed temperatures. The magnitude of the water flux associated with hyporheic exchange can either increase or decrease with stream discharge, depending primarily on channel morphology (Buffington & Tonina, 2009; Tonina & Buffington, 2009). However, even if hyporheic exchange flow increases with stream discharge,

the influence on stream temperature may be limited since the ratio of hyporheic exchange flow to streamflow can still be low (Wondzell, 2011). During high flows, as well as during winter periods, stream and bed temperatures can be similar, which will also limit the magnitude of the hyporheic heat exchange regardless of whether a large proportion of water is exchanging with the hyporheic zone (Leach & Moore, 2014).

3.3.3 | Friction

Friction adds heat to the stream due to the dissipation of both gravitational potential energy associated with changes in elevation and turbulent kinetic energy associated with instream flow (Meier et al., 2003). The magnitude of the friction flux is a function of channel slope and stream velocity, with steeper channels and higher velocity resulting in greater flux magnitudes (Theurer et al., 1984). Compared to the other fluxes, friction has received limited detailed examination. The friction flux is typically only a small component in most stream energy balances and is often assumed to be negligible, especially for low-gradient channels (Garner et al., 2015; Webb & Zhang, 1997). However, this flux can be an important energy source relative to other fluxes for steep mountainous stream channels with high flows (Magnusson et al., 2012; Meier et al., 2003).

4 | STREAM ENERGY BALANCE FOR A FORESTED RAIN-DOMINATED CATCHMENT

This section presents an idealized schema of how the stream energy balance varies both seasonally and with stream size for a forested catchment with a coastal temperate or Mediterranean climate, with warm, dry summers and cool, wet winters dominated by rainfall, as typified by coastal regions of the Pacific Northwest of North America (Figure 4). The

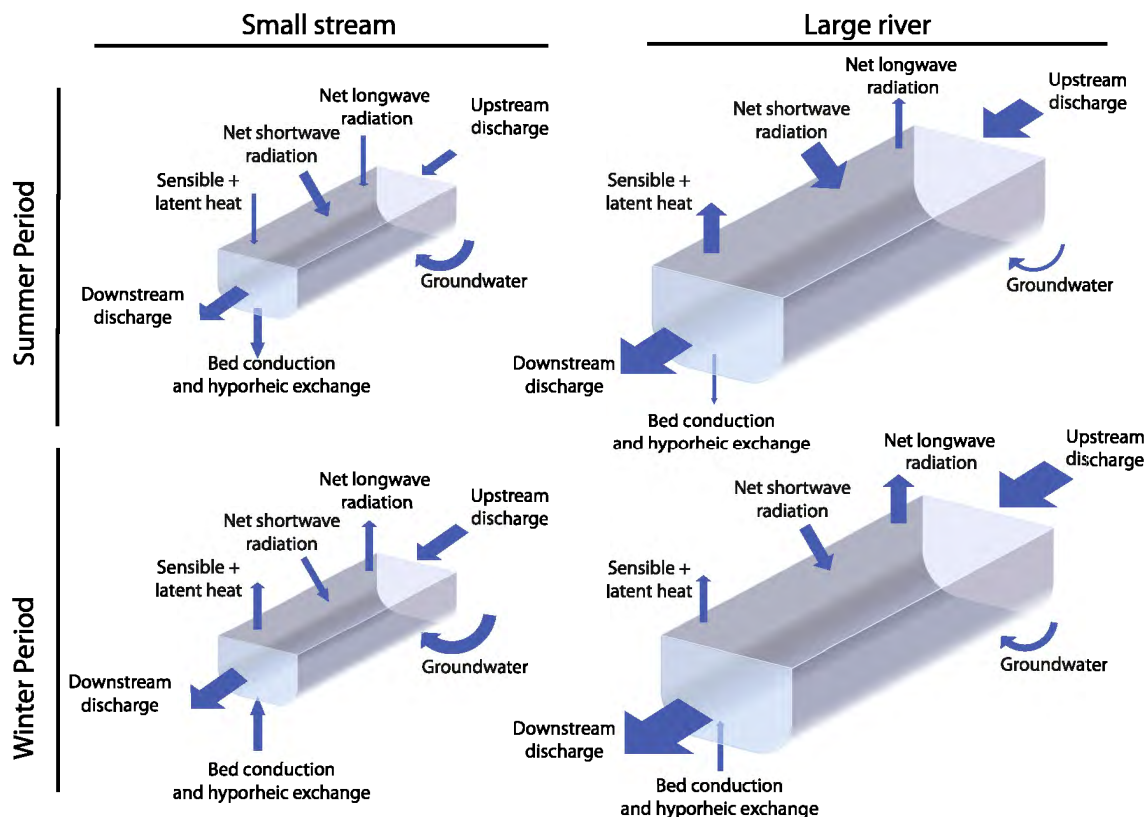


FIGURE 4 Conceptual energy balance for a small headwater stream and a large (e.g., fifth order or higher) river during summer and winter. The arrowhead represents the net seasonal direction of the energy flux, and the size of the arrow is scaled to its relative importance to the overall reach-scale energy balance. The hypothetical energy balances represent forested streams with extensive riparian vegetation characterized by a Mediterranean climate (warm and dry summers and wet and cool winters with precipitation falling primarily as rain).

streamflow regime is dominated by rainfall-generated high flows in winter and low flows during summer. We selected this environment as a case example due to the background of research available to support a synthesis (Brown, 1969; Johnson, 2004; Leach & Moore, 2014; Moore, Spittlehouse, et al., 2005).

In summer, the energy balance of the small headwater stream will be dominated by heat inputs associated with net radiation and advection from subsurface inflow. Even with extensive shade, a portion of the incoming solar radiation, which is elevated during summer, will reach the stream surface. In addition, the above-stream forest cover will (1) reduce ventilation, thereby suppressing sensible and latent heat exchange, and (2) elevate incoming longwave radiation due to significant canopy cover and higher emissivity of vegetation compared to the atmosphere. The air and vegetation canopy above the stream will generally be warmer than the stream during the day, which will cause the net longwave and sensible fluxes to be heat sources to the stream (Story et al., 2003). These heat inputs will typically be partially offset by evaporative losses from the stream surface. During these low-flow summer periods, the water in the stream will be primarily sourced from groundwater or hillslope discharge. Discharge will be relatively low compared to high flow periods during winter (Leach & Moore, 2014). Heat transfer into the bed via conduction and hyporheic exchange will be the dominant heat loss, in part because the magnitudes of the other fluxes will be relatively low.

For the large river, net shortwave radiation will be the largest heat source during summer due to the limited shading influence of riparian vegetation, topography, or both (Webb & Zhang, 1997). Net longwave radiation will be a minor term since incoming and outgoing longwave radiation will be of similar magnitude. The incoming longwave radiation flux will be lower than for the small stream due to the large sky view factor and low emissivity of the atmosphere. In addition, outgoing longwave radiation will be greater and more stable compared to the small stream since the water temperature will be higher and show less diel variability. Since the river surface is more exposed, high winds will promote the sensible and latent heat fluxes, and evaporation can be a key heat loss. Groundwater and hyporheic exchange will be minor terms in the energy balance of the large river since the relative discharges of these hydrologic inflows will be substantially smaller than in-stream discharge. Bed conduction will be a heat loss as the stream will be warmer than the subsurface, but a small component of the energy balance compared to the surface energy flux magnitudes.

Winter conditions will be characterized by higher stream discharge, low solar radiation (regardless of stream canopy cover), and air temperature that is typically lower than stream temperature. For the small stream, this will mean that net longwave radiation, as well as sensible and latent heat, will transfer heat away from the stream. This will be the same for the large river; however, the net longwave radiation flux will be a greater heat loss because the large river will receive less incoming longwave radiation than the small stream. This difference in incoming longwave radiation is due to the greater canopy cover for the small stream, which has higher emissivity compared to the atmosphere. Since there will be greater subsurface flow and stream discharge due to wetter winter conditions, advection associated with upstream discharge and groundwater inflow will be major components of the energy balance. Energy transfer at the stream–bed interface will consist of a minor heat input to both the small stream and large river due to the sediments below the streambed being generally warmer than the stream.

This simplified seasonal energy balance for small streams and large rivers in a forested, rain-dominated Mediterranean climate helps illustrate key differences in the various energy exchange processes. Streams in other landscapes with different climate, hydrology, geology, vegetation, and anthropogenic influences, such as dams, industrial water withdrawals, and effluent, will be characterized by energy exchanges differing in magnitude and direction, both seasonally and across spatial scales. We focused on net seasonal fluxes in our case, and readers interested in diel patterns in stream energy budgets are referred to examples from other papers (e.g., Brown, 1969; Hebert et al., 2011; Webb & Zhang, 1997). Researchers and practitioners can draw upon the qualitative descriptions of energy fluxes and their controlling factors presented in this paper to conceptualize which fluxes control their system of interest, how these fluxes might respond to environmental or management changes, and to inform observational and modeling strategies.

5 | CONCLUSION

The thermal regime of a stream is the result of complex energy exchange processes, the magnitude and direction of which vary in space and time. Stream energy processes can be organized as stream surface energy exchanges (solar and longwave radiation, and sensible and latent heat fluxes), streambed exchanges (bed conduction, hyporheic exchange, and friction), and advective exchanges associated with hydrologic processes (surface and subsurface inflows, industrial effluent and water withdrawals, and in-channel flows). The importance of solar radiation is well recognized; however, other processes, in particular advective exchanges, can be critical controls on stream temperature at a range of spatial and temporal scales. An energy and water balance approach is an effective and transferable framework for investigating

and understanding the dominant energy exchanges driving stream thermal regimes and their response to environmental and anthropogenic changes. Practitioners and researchers in a range of fields concerned about stream temperature will benefit from applying this conceptual framework to their stream systems.

AUTHOR CONTRIBUTIONS

Jason Leach: Conceptualization (lead); visualization (equal); writing – original draft (lead); writing – review and editing (equal). **Christa Kelleher:** Conceptualization (supporting); visualization (equal); writing – review and editing (equal). **Barret L. Kurylyk:** Conceptualization (supporting); visualization (supporting); writing – review and editing (equal). **R. Dan Moore:** Conceptualization (supporting); visualization (supporting); writing – review and editing (equal). **Bethany Neilson:** Conceptualization (equal); visualization (supporting); writing – review and editing (equal).

ACKNOWLEDGMENTS

Figure 1 was illustrated by J. Spahr Scientific Visualization (www.scivisuals.com). We thank Danielle Hudson for providing feedback on an earlier version of the manuscript. We also thank two anonymous reviewers who provided valuable feedback that improved the manuscript.

FUNDING INFORMATION

Funding support was provided by a NSERC Discovery Grant to JAL and the Canadian Forest Service's Sustainable Forest Management Program.

CONFLICT OF INTEREST STATEMENT

The authors have declared no conflicts of interest for this article.

DATA AVAILABILITY STATEMENT

Data sharing is not applicable to this article as no new data were created or analyzed in this study.

ORCID

Jason A. Leach  <https://orcid.org/0000-0001-6639-7993>

REFERENCES

- Anderson, E. R. (1954). Water-loss investigations: Lake Hefner studies. Energy-budget studies. Technical report, U.S. Technical report, Professional Paper 269. Geological Survey. US Department of Interior, Washington, DC.
- Arismendi, I., Safeeq, M., Dunham, J. B., & Johnson, S. L. (2014). Can air temperature be used to project influences of climate change on stream temperature? *Environmental Research Letters*, 9(8), 084015.
- Armstrong, J. B., Fullerton, A. H., Jordan, C. E., Ebersole, J. L., Bellmore, J. R., Arismendi, I., Penaluna, B. E., & Reeves, G. H. (2021). The importance of warm habitat to the growth regime of cold-water fishes. *Nature Climate Change*, 11(4), 354–361.
- Arrigoni, A., Poole, G., Mertes, L., O'Daniel, S., Woessner, W., & Thomas, S. (2008). Buffered, lagged, or cooled? Disentangling hyporheic influences on temperature cycles in stream channels. *Water Resources Research*, 44(9), W09418.
- Arscott, D., Tockner, K., & Ward, J. (2001). Thermal heterogeneity along a braided floodplain river (Tagliamento River, northeastern Italy). *Canadian Journal of Fisheries and Aquatic Sciences*, 58(12), 2359–2373.
- Aubry-Wake, C., Bertocini, A., & Pomeroy, J. W. (2022). Fire and ice: The impact of wildfire-affected albedo and irradiance on glacier melt. *Earth's Futures*, 10(4), e2022EF002685.
- Benner, D. A. (2000). Evaporative heat loss of the upper middle fork of the John Day River, northeastern Oregon (Master's thesis).
- Benyahya, L., Caissie, D., El-Jabi, N., & Satish, M. (2010). Comparison of microclimate vs. remote meteorological data and results applied to a water temperature model (Miramichi River, Canada). *Journal of Hydrology*, 380, 247–259.
- Benyahya, L., Caissie, D., Satish, M. G., & El-Jabi, N. (2012). Long-wave radiation and heat flux estimates within a small tributary in catamaran brook (New Brunswick, Canada). *Hydrological Processes*, 26, 475–484.
- Boano, F., Harvey, J. W., Marion, A., Packman, A. I., Revelli, R., Ridolfi, L., & Wörman, A. (2014). Hyporheic flow and transport processes: Mechanisms, models, and biogeochemical implications. *Reviews of Geophysics*, 52(4), 603–679.
- Bray, E. N., Dozier, J., & Dunne, T. (2017). Mechanics of the energy balance in large lowland rivers, and why the bed matters. *Geophysical Research Letters*, 44(17), 8910–8918.
- Briggs, M. A., & Hare, D. K. (2018). Explicit consideration of preferential groundwater discharges as surface water ecosystem control points. *Hydrological Processes*, 32(15), 2435–2440.

- Briggs, M. A., Johnson, Z. C., Snyder, C. D., Hitt, N. P., Kurylyk, B. L., Lautz, L., Irvine, D. J., Hurley, S. T., & Lane, J. W. (2018). Inferring watershed hydraulics and cold-water habitat persistence using multi-year air and stream temperature signals. *Science of the Total Environment*, 636, 1117–1127.
- Brown, G. (1969). Predicting temperatures of small streams. *Water Resources Research*, 5(1), 68–75.
- Brown, G. W., & Krygier, J. T. (1970). Effects of clear-cutting on stream temperature. *Water Resources Research*, 6(4), 1133–1139.
- Brown, L. E., & Hannah, D. M. (2007). Alpine stream temperature response to storm events. *Journal of Hydrometeorology*, 8(4), 952–967.
- Brown, L. E., & Hannah, D. M. (2008). Spatial heterogeneity of water temperature across an alpine river basin. *Hydrological Processes*, 22(7), 954–967.
- Buffington, J. M., & Tonina, D. (2009). Hyporheic exchange in mountain rivers II: Effects of channel morphology on mechanics, scales, and rates of exchange. *Geography Compass*, 3(3), 1038–1062.
- Caissie, D. (2006). The thermal regime of rivers: A review. *Freshwater Biology*, 51(8), 1389–1406.
- Caissie, D. (2016). River evaporation, condensation and heat fluxes within a first-order tributary of catamaran brook (New Brunswick, Canada). *Hydrological Processes*, 30(12), 1872–1883.
- Caissie, D., Kurylyk, B. L., St-Hilaire, A., El-Jabi, N., & MacQuarrie, K. T. B. (2014). Streambed temperature dynamics and corresponding heat fluxes in small streams experiencing seasonal ice cover. *Journal of Hydrology*, 519, 1441–1452.
- Caissie, D., & Luce, C. H. (2017). Quantifying streambed advection and conduction heat fluxes. *Water Resources Research*, 53(2), 1595–1624.
- Caissie, D., Satish, M. G., & El-Jabi, N. (2007). Predicting water temperatures using a deterministic model: Application on Miramichi River catchments (New Brunswick, Canada). *Journal of Hydrology*, 336, 303–315.
- Cardenas, M. B. (2015). Hyporheic zone hydrologic science: A historical account of its emergence and a prospectus. *Water Resources Research*, 51(5), 3601–3616.
- Cardenas, M. B., Doering, M., Rivas, D. S., Galdeano, C., Neilson, B. T., & Robinson, C. T. (2014). Analysis of the temperature dynamics of a proglacial river using time-lapse thermal imaging and energy balance modeling. *Journal of Hydrology*, 519, 1963–1973.
- Constantz, J. (1998). Interaction between stream temperature, streamflow, and groundwater exchanges in alpine streams. *Water Resources Research*, 34(7), 1609–1615.
- David, A. T., Asarian, J. E., & Lake, F. K. (2018). Wildfire smoke cools summer river and stream water temperatures. *Water Resources Research*, 54(10), 7273–7290.
- Delpla, I., Jung, A.-V., Baures, E., Clement, M., & Thomas, O. (2009). Impacts of climate change on surface water quality in relation to drinking water production. *Environment International*, 35(8), 1225–1233.
- Demars, B. O., Russell Manson, J., Olafsson, J. S., Gislason, G. M., Gudmundsdottir, R., Woodward, G., Reiss, J., Pichler, D. E., Rasmussen, J. J., & Friberg, N. (2011). Temperature and the metabolic balance of streams. *Freshwater Biology*, 56(6), 1106–1121.
- Devito, K., Creed, I., Gan, T., Mendoza, C., Petrone, R., Silins, U., & Smerdon, B. (2005). A framework for broad-scale classification of hydrologic response units on the boreal plain: Is topography the last thing to consider? *Hydrological Processes*, 19(8), 1705–1714.
- Dibble, K. L., Yackulic, C. B., Kennedy, T. A., Bestgen, K. R., & Schmidt, J. C. (2021). Water storage decisions will determine the distribution and persistence of imperiled river fishes. *Ecological Applications*, 31(2), e02279.
- Dugdale, S. J., Hannah, D. M., & Malcolm, I. A. (2017). River temperature modelling: A review of process-based approaches and future directions. *Earth-Science Reviews*, 175, 97–113.
- Dugdale, S. J., Kelleher, C. A., Malcolm, I. A., Caldwell, S., & Hannah, D. M. (2019). Assessing the potential of drone-based thermal infrared imagery for quantifying river temperature heterogeneity. *Hydrological Processes*, 33(7), 1152–1163.
- Dunham, J. B., Rosenberger, A. E., Luce, C. H., & Rieman, B. E. (2007). Influences of wildfire and channel reorganization on spatial and temporal variation in stream temperature and the distribution of fish and amphibians. *Ecosystems*, 10(2), 335–346.
- Ebersole, J. L., Liss, W. J., & Frissell, C. A. (2001). Relationship between stream temperature, thermal refugia and rainbow trout (*Oncorhynchus mykiss*) abundance in arid-land streams in the northwestern United States. *Ecology of Freshwater Fish*, 10(1), 1–10.
- Evans, E., McGregor, G., & Petts, G. (1998). River energy budgets with special reference to river bed processes. *Hydrological Processes*, 12(4), 575–595.
- Findlay, S. (1995). Importance of surface-subsurface exchange in stream ecosystems: The hyporheic zone. *Limnology and Oceanography*, 40(1), 159–164.
- Fullerton, A. H., Torgersen, C. E., Lawler, J. J., Faux, R. N., Steel, E. A., Beechie, T. J., Ebersole, J. L., & Leibowitz, S. G. (2015). Rethinking the longitudinal stream temperature paradigm: Region-wide comparison of thermal infrared imagery reveals unexpected complexity of river temperatures. *Hydrological Processes*, 29(22), 4719–4737.
- Garner, G., Malcolm, I. A., Sadler, J., & Hannah, D. (2014). What causes cooling water temperature gradients in a forested stream reach? *Hydrology and Earth System Sciences*, 18(12), 5361–5376.
- Garner, G., Malcolm, I. A., Sadler, J. P., Millar, C. P., & Hannah, D. H. (2015). Inter-annual variability in the effects of riparian woodland on micro-climate, energy exchanges and water temperature of an upland Scottish stream. *Hydrological Processes*, 29, 1080–1095.
- Gu, R., Montgomery, S., & Austin, T. A. (1998). Quantifying the effects of stream discharge on summer river temperature. *Hydrological Sciences Journal*, 43(6), 885–904.
- Guenther, S. M., Gomi, T., & Moore, R. D. (2014). Stream and bed temperature variability in a coastal headwater catchment: Influences of surface-subsurface interactions and partial-retention forest harvesting. *Hydrological Processes*, 28, 1238–1249.
- Guenther, S. M., Moore, R. D., & Gomi, T. (2012). Riparian microclimate and evaporation from a coastal headwater stream and their response to partial-retention forest harvesting. *Agriculture and Forest Meteorology*, 164, 1–9.

- Gulliver, J. S., & Stefan, H. G. (1986). Wind function for a sheltered stream. *Journal of Environmental Engineering*, 112(2), 387–399.
- Hannah, D. M., & Garner, G. (2015). River water temperature in the United Kingdom: Changes over the 20th century and possible changes over the 21st century. *Progress in Physical Geography*, 39(1), 68–92.
- Hannah, D. M., Malcolm, I. A., Soulsby, C., & Youngson, A. F. (2008). A comparison of forest and moorland stream microclimate, heat exchanges and thermal dynamics. *Hydrological Processes*, 22(7), 919–940.
- Hare, D. K., Helton, A. M., Johnson, Z. C., Lane, J. W., & Briggs, M. A. (2021). Continental-scale analysis of shallow and deep groundwater contributions to streams. *Nature Communications*, 12(1), 1–10.
- Hayes, N. M., Deemer, B. R., Corman, J. R., Razavi, N. R., & Strock, K. E. (2017). Key differences between lakes and reservoirs modify climate signals: A case for a new conceptual model. *Limnology and Oceanography Letters*, 2(2), 47–62.
- Heavilin, J., & Neilson, B. T. (2012). Approximation of inverse Laplace transform solution to heat transport in a stream system. *Water Resources Research*, 48(9), W09603.
- Hebert, C., Caissie, D., Satish, M. G., & El-Jabi, N. (2011). Study of stream temperature dynamics and corresponding heat fluxes within Miramichi River catchments (New Brunswick, Canada). *Hydrological Processes*, 25, 2439–2455.
- Held, I. M., & Soden, B. J. (2000). Water vapor feedback and global warming. *Annual Review of Energy and the Environment*, 25(1), 441–475.
- Isaak, D. J., Wenger, S. J., Peterson, E. E., Ver Hoef, J. M., Nagel, D. E., Luce, C. H., Hostetler, S. W., Dunham, J. B., Roper, B. B., Wollrab, S. P., Chandler, G. L., Horan, D. L., & Parkes-Payne, S. (2017). The NorWeST summer stream temperature model and scenarios for the Western U.S.: A crowd-sourced database and new geospatial tools Foster a user community and predict broad climate warming of Rivers and streams. *Water Resources Research*, 53, 9181–9205.
- Jankowski, K., & Schindler, D. (2019). Watershed geomorphology modifies the sensitivity of aquatic ecosystem metabolism to temperature. *Scientific Reports*, 9(1), 17619.
- Johnson, S. L. (2003). Stream temperature: Scaling of observations and issues for modelling. *Hydrological Processes*, 17(2), 497–499.
- Johnson, S. L. (2004). Factors influencing stream temperatures in small streams: Substrate effects and a shading experiment. *Canadian Journal of Fisheries and Aquatic Sciences*, 61(6), 913–923.
- Johnston, S. G., Karimian, N., & Burton, E. D. (2020). Seasonal temperature oscillations drive contrasting arsenic and antimony mobilization in a mining-impacted river system. *Water Resources Research*, 56(10), e2020WR028196.
- Jones, N. E. (2010). Incorporating lakes within the river discontinuum: Longitudinal changes in ecological characteristics in stream-lake networks. *Canadian Journal of Fisheries and Aquatic Sciences*, 67(8), 1350–1362.
- Kelleher, C., Wagener, T., Gooseff, M., McGlynn, B., McGuire, K., & Marshall, L. (2012). Investigating controls on the thermal sensitivity of Pennsylvania streams. *Hydrological Processes*, 26(5), 771–785.
- King, T. V., & Neilson, B. T. (2019). Quantifying reach-average effects of hyporheic exchange on Arctic river temperatures in an area of continuous permafrost. *Water Resources Research*, 55(3), 1951–1971.
- Kirk, J. T. (2011). *Light and photosynthesis in aquatic ecosystems* (3rd ed.). Cambridge University Press.
- Klos, P. Z., & Link, T. E. (2018). Quantifying shortwave and longwave radiation inputs to headwater streams under differing canopy structures. *Forest Ecology and Management*, 407, 116–124.
- Kobayashi, D. (1985). Separation of the snowmelt hydrograph by stream temperatures. *Journal of Hydrology*, 76(1), 155–162.
- Kobayashi, D., Ishii, Y., & Nomura, M. (1994). Comparison of stream temperatures during stormflow from snowmelt and rainfall and hydrograph separation. *Journal of Japan Society of Hydrology and Water Resources*, 7(6), 512–519.
- Kurylyk, B. L., MacQuarrie, K. T., Caissie, D., & McKenzie, J. M. (2015). Shallow groundwater thermal sensitivity to climate change and land cover disturbances: Derivation of analytical expressions and implications for stream temperature modeling. *Hydrology and Earth System Sciences*, 19(5), 2469–2489.
- Kurylyk, B. L., MacQuarrie, K. T., & McKenzie, J. M. (2014). Climate change impacts on groundwater and soil temperatures in cold and temperate regions: Implications, mathematical theory, and emerging simulation tools. *Earth-Science Reviews*, 138, 313–334.
- Kurylyk, B. L., MacQuarrie, K. T. B., & Voss, C. I. (2014). Climate change impacts on the temperature and magnitude of groundwater discharge from shallow, unconfined aquifers. *Water Resources Research*, 50, 3253–3274.
- Kurylyk, B. L., Moore, R. D., & MacQuarrie, K. T. B. (2016). Scientific briefing: Quantifying streambed head advection associated with groundwater-surface water interactions. *Hydrological Processes*, 30, 978–992.
- Lapham, W. W. (1989). Use of temperature profiles beneath streams to determine rates of vertical ground-water flow and vertical hydraulic conductivity. Technical report, USGS water-supply paper 2337, 35 p.
- Leach, J. A., Lidberg, W., Kuglerová, L., Peralta-Tapia, A., Ågren, A., & Laudon, H. (2017). Evaluating topography-based predictions of shallow lateral groundwater discharge zones for a boreal lake–stream system. *Water Resources Research*, 53, 5420–5437.
- Leach, J. A., & Moore, R. D. (2010). Above-stream microclimate and stream surface energy exchanges in a wildfire-disturbed riparian zone. *Hydrological Processes*, 24(17), 2369–2381.
- Leach, J. A., & Moore, R. D. (2011). Stream temperature dynamics in two hydrogeomorphically distinct reaches. *Hydrological Processes*, 25(5), 679–690.
- Leach, J. A., & Moore, R. D. (2014). Winter stream temperature in the rain-on-snow zone of the Pacific northwest: Influences of hillslope runoff and transient snow cover. *Hydrology and Earth System Sciences*, 18, 819–838.
- Leach, J. A., & Moore, R. D. (2017). Insights on stream temperature processes through development of a coupled hydrologic and stream temperature model for forested coastal headwater catchments. *Hydrological Processes*, 31, 3160–3177.

- Leach, J. A., & Moore, R. D. (2019). Empirical stream thermal sensitivities may underestimate stream temperature response to climate warming. *Water Resources Research*, *55*(7), 5453–5467.
- Leach, J. A., Neilson, B., Buahin, C., Moore, R. D., & Laudon, H. (2021). Lake outflow and hillslope lateral inflows dictate thermal regimes of forested streams draining small lakes. *Water Resources Research*, *57*, e2020WR028136.
- Lisi, P. J., Schindler, D. E., Cline, T. J., Scheuerell, M. D., & Walsh, P. B. (2015). Watershed geomorphology and snowmelt control stream thermal sensitivity to air temperature. *Geophysical Research Letters*, *42*(9), 3380–3388.
- Luce, C., Staab, B., Kramer, M., Wenger, S., Isaak, D., & McConnell, C. (2014). Sensitivity of summer stream temperatures to climate variability in the Pacific northwest. *Water Resources Research*, *50*(4), 3428–3443.
- MacDonald, R. J., Boon, S., Byrne, J. M., & Silins, U. (2014). A comparison of surface and subsurface controls on summer temperature in a headwater stream. *Hydrological Processes*, *28*, 2338–2347.
- Magnusson, J., Jonas, T., & Kirchner, J. W. (2012). Temperature dynamics of a proglacial stream: Identifying dominant energy balance components and inferring spatially integrated hydraulic geometry. *Water Resources Research*, *48*(6), W06510.
- Maheu, A., Caissie, D., St-Hilaire, A., & El-Jabi, N. (2014). River evaporation and corresponding heat fluxes in forested catchments. *Hydrological Processes*, *28*(23), 5725–5738.
- Maheu, A., St-Hilaire, A., Caissie, D., El-Jabi, N., Bourque, G., & Boisclair, D. (2016). A regional analysis of the impact of dams on water temperature in medium-size rivers in eastern Canada. *Canadian Journal of Fisheries and Aquatic Sciences*, *73*(12), 1885–1897.
- Majerova, M., Neilson, B. T., & Roper, B. B. (2020). Beaver dam influences on streamflow hydraulic properties and thermal regimes. *Science of the Total Environment*, *718*, 134853.
- McMahon, A., & Moore, R. D. (2017). Influence of turbidity and aeration on the albedo of mountain streams. *Hydrological Processes*, *31*(25), 4477–4491.
- Meier, W., Bonjour, C., Wüest, A., & Reichert, P. (2003). Modeling the effect of water diversion on the temperature of mountain streams. *Journal of Environmental Engineering*, *129*(8), 755–764.
- Menberg, K., Blum, T., Kurylyk, B. L., & Bayer, P. (2014). Observed groundwater temperature response to recent climate change. *Hydrology and Earth System Sciences*, *11*, 3637–3673.
- Mihalevich, B. A., Neilson, B. T., Buahin, C. A., Yackulic, C. B., & Schmidt, J. C. (2020). Water temperature controls for regulated canyon-bound rivers. *Water Resources Research*, *56*, e2020WR027566.
- Mohseni, O., Stefan, H. G., & Erickson, T. R. (1998). A nonlinear regression model for weekly stream temperatures. *Water Resources Research*, *34*, 2685–2692.
- Moore, R. D., & Leach, J. A. (2021). Predicting latent and sensible heat fluxes in stream temperature models: Current challenges and potential solutions. *Water Resources Research*, *57*(2), e2020WR028712.
- Moore, R. D., Spittlehouse, D. L., & Story, A. (2005). Riparian microclimate and stream temperature response to forest harvesting: A review. *Journal of the American Water Resources Association*, *41*(4), 813–834.
- Moore, R. D., Sutherland, P., Gomi, T., & Dhakal, A. (2005). Thermal regime of a headwater stream within a clear-cut, coastal British Columbia, Canada. *Hydrological Processes*, *19*(13), 2591–2608.
- Neilson, B. T., Chapra, S., Stevens, D. K., & Bandaragoda, C. (2010). Two-zone transient storage modeling using temperature and solute data with multiobjective calibration: 1. Temperature. *Water Resources Research*, *46*(12), W12520.
- Neilson, B. T., Hatch, C. E., Ban, H., & Tyler, S. W. (2010). Solar radiative heating of fiber-optic cables used to monitor temperatures in water. *Water Resources Research*, *46*(8), W08540.
- Neilson, B. T., Stevens, D. K., Chapra, S. C., & Bandaradoga, C. (2009). Data collection methodology for dynamic temperature model testing and corroboration. *Hydrological Processes*, *23*(20), 2902–2914.
- Nelson, K. C., & Palmer, M. A. (2007). Stream temperature surges under urbanization and climate change: Data, models, and responses. *Journal of the American Water Resources Association*, *43*(2), 440–452.
- Oke, T. (1987). *Boundary layer climates* (2nd ed.). Halsted Press.
- Olden, J. D., & Naiman, R. J. (2010). Incorporating thermal regimes into environmental flows assessments: Modifying dam operations to restore freshwater ecosystem integrity. *Freshwater Biology*, *55*(1), 86–107.
- Ouellet, V., St-Hilaire, A., Dugdale, S. J., Hannah, D. M., Krause, S., & Proulx-Ouellet, S. (2020). River temperature research and practice: Recent challenges and emerging opportunities for managing thermal habitat conditions in stream ecosystems. *Science of the Total Environment*, *736*, 139679.
- Poole, G. C., & Berman, C. H. (2001). An ecological perspective on in-stream temperature: Natural heat dynamics and mechanisms of human-caused thermal degradation. *Environmental Management*, *27*(6), 787–802.
- Richards, J., & Moore, R. D. (2011). Discharge dependence of stream albedo in a steep proglacial channel. *Hydrological Processes*, *25*(26), 4154–4158.
- Richards, J., Moore, R. D., & Forrest, A. (2012). Late-summer thermal regime of a small proglacial lake. *Hydrological Processes*, *26*(18), 2687–2695.
- Risley, J. C., Constantz, J., Essaid, H., & Rounds, S. (2010). Effects of upstream dams versus groundwater pumping on stream temperature under varying climate conditions. *Water Resources Research*, *46*, W06517.
- Roesky, B., & Hayashi, M. (2022). Effects of lake-groundwater interaction on the thermal regime of a sub-alpine headwater stream. *Hydrological Processes*, *36*(2), e14501.

- Rutherford, J. C., Blackett, S., Blackett, C., Saito, L., & Davies-Colley, R. J. (1997). Predicting the effects of shade on water temperature in small streams. *New Zealand Journal of Marine and Freshwater Research*, 31(5), 707–721.
- Sanroma, E., Palle, E., & Sanchez-Lorenzo, A. (2010). Long-term changes in insolation and temperatures at different altitudes. *Environmental Research Letters*, 5(2), 024006.
- Saur, J., & Anderson, E. (1956). The heat budget of a body of water of varying volume. *Limnology and Oceanography*, 1(4), 247–251.
- Schliemann, S. A., Grevstad, N., & Brazeau, R. H. (2021). Water quality and spatio-temporal hot spots in an effluent-dominated urban river. *Hydrological Processes*, 35(1), e14001.
- Schmadel, N. M., Neilson, B. T., & Heavilin, J. E. (2015). Spatial considerations of stream hydraulics in reach scale temperature modeling. *Water Resources Research*, 51(7), 5566–5581.
- Shanley, J., & Peters, N. (1988). Preliminary observations of streamflow generation during storms in a forested Piedmont watershed using temperature as a tracer. *Journal of Contaminant Hydrology*, 3(2–4), 349–365.
- Sinokrot, B., & Stefan, H. (1993). Stream temperature dynamics: Measurements and modeling. *Water Resources Research*, 29(7), 2299–2312.
- Sridhar, V., Sansone, A. L., LaMarche, J., Dubin, T., & Lettenmaier, D. P. (2004). Prediction of stream temperature in forested watersheds. *Journal of the American Water Resources Association*, 40(1), 197–213.
- Steel, E. A., Beechie, T. J., Torgersen, C. E., & Fullerton, A. H. (2017). Envisioning, quantifying, and managing thermal regimes on river networks. *Bioscience*, 67(6), 506–522.
- St-Hilaire, A., Morin, G., El-Jabi, N., & Caissie, D. (2000). Water temperature modelling in a small forested stream: Implications of forest canopy and soil temperatures. *Canadian Journal of Civil Engineering*, 27(6), 1095–1108.
- Story, A., Moore, R. D., & Macdonald, J. S. (2003). Stream temperatures in two shaded reaches below cutblocks and logging roads: Downstream cooling linked to subsurface hydrology. *Canadian Journal of Forest Research*, 33(8), 1383–1396.
- Sturrock, A., Winter, T., & Rosenberry, D. (1992). Energy budget evaporation from Williams Lake: A closed lake in north Central Minnesota. *Water Resources Research*, 28(6), 1605–1617.
- Theurer, F. D., Voos, K. A., & Miller, W. J. (1984). Instream water temperature model. Technical report, Fort Collins, CO: Fish and wildlife service instream flow information paper 16, FWS/OBS-84/15, 335 p.
- Tonina, D., & Buffington, J. M. (2009). Hyporheic exchange in mountain rivers I: Mechanics and environmental effects. *Geography Compass*, 3(3), 1063–1086.
- Torgersen, C. E., Price, D. M., Li, H. W., & McIntosh, B. A. (1999). Multiscale thermal refugia and stream habitat associations of Chinook salmon in northeastern Oregon. *Ecological Applications*, 9(1), 301–319.
- Troxler, R. W., & Thackston, E. L. (1977). Predicting the rate of warming of rivers below hydroelectric installations. *Journal of Water Pollution Control Federation*, 49, 1902–1912.
- van Vliet, M. T., Yearsley, J. R., Ludwig, F., Vögele, S., Lettenmaier, D. P., & Kabat, P. (2012). Vulnerability of US and European electricity supply to climate change. *Nature Climate Change*, 2(9), 676–681.
- Verpoorter, C., Kutser, T., Seekell, D. A., & Tranvik, L. J. (2014). A global inventory of lakes based on high-resolution satellite imagery. *Geophysical Research Letters*, 41(18), 6396–6402.
- Vugts, H. (1974). Calculation of temperature variations of small mountain streams. *Journal of Hydrology*, 23, 267–278.
- Wankiewicz, A. (1984). Analysis of winter heat flow in an ice-covered Arctic stream. *Canadian Journal of Civil Engineering*, 11(3), 430–443.
- Ward, A. S. (2016). The evolution and state of interdisciplinary hyporheic research. *WIREs Water*, 3(1), 83–103.
- Webb, B., Hannah, D. M., Moore, R. D., Brown, L. E., & Nobilis, F. (2008). Recent advances in stream and river temperature research. *Hydrological Processes*, 22(7), 902–918.
- Webb, B., & Zhang, Y. (1997). Spatial and seasonal variability in the components of the river heat budget. *Hydrological Processes*, 11(1), 79–101.
- Webb, B. W., & Zhang, Y. (1999). Water temperatures and heat budgets in Dorset chalk water courses. *Hydrological Processes*, 13(3), 309–321.
- Wehrly, K. E., Wiley, M. J., & Seelbach, P. W. (2006). Influence of landscape features on summer water temperatures in lower Michigan streams. *American Fisheries Society Symposium*, 48, 113–127.
- West, D. T., & Moore, R. D. (2020). Influences of upstream reservoir stratification and downstream tidal fluctuations on the summer thermal regime of a regulated coastal river. *Hydrological Processes*, 34, 4660–4674.
- Wild, M., Gilgen, H., Roesch, A., Ohmura, A., Long, C. N., Dutton, E. G., Forgan, B., Kallis, A., Russak, V., & Tsvetkov, A. (2005). From dimming to brightening: Decadal changes in solar radiation at earth's surface. *Science*, 308(5723), 847–850.
- Wondzell, S. M. (2011). The role of the hyporheic zone across stream networks. *Hydrological Processes*, 25(22), 3525–3532.
- Xin, Z., & Kinouchi, T. (2013). Analysis of stream temperature and heat budget in an urban river under strong anthropogenic influences. *Journal of Hydrology*, 489, 16–25.

How to cite this article: Leach, J. A., Kelleher, C., Kurylyk, B. L., Moore, R. D., & Neilson, B. T. (2023). A primer on stream temperature processes. *WIREs Water*, 10(4), e1643. <https://doi.org/10.1002/wat2.1643>

Technical Memorandum

To:	Gene Bosley, P.E.	Project:	Stibnite Gold Project
From:	Kevin Jensen, P.E.	cc:	File
Date:	December 9, 2022	Job No.:	22-095
Subject:	Supplemental Tunnel Hydraulic Modeling		

Revision No.	Date	Description
0	09/02/2022	Initial draft
1	10/03/2022	Revised draft based on Perpetua Resources comments
2	11/12/2022	Final draft based on Perpetua Resources comments
3	12/09/2022	Final

1.0 Introduction

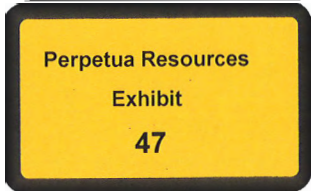
This Technical Memorandum (TM) provides supplemental hydraulic modeling results evaluating low-flow performance of the proposed tunnel fishway for Perpetua Resources Idaho, Inc.’s (Perpetua’s) Stibnite Gold Project (Project). Section 1 presents the Project overview, including background, task description, purpose, and design criteria adopted in previous Project-related research. Sections 2 and 3 introduce hydraulic calculations and modeling for evaluating weir flow in the fishway, respectively. Conclusions are provided in Section 4.

1.1 Background and Purpose

1.1.1 Project Background

Perpetua intends to re-open and expand the Stibnite Mine leading to eventual restoration and closure. In accordance with the mine development plan, the East Fork South Fork Salmon River (EFSFSR) must be diverted through a tunnel around the Yellow Pine pit (YPP). The EFSFSR Diversion Tunnel is a critical component of the successful development of the Stibnite Gold Project.

McMillen Jacobs Associates (2017; 2018; 2019) previously performed the preliminary tunnel design, including tunnel routing, hydraulic analysis, and civil design, to support the inclusion of an in-tunnel fishway. The previous study introduced hydraulic modeling using a Computational Fluid Dynamics (CFD) model.



1.2 Project Description

The location of the Project is approximately 10 miles east of the town of Yellow Pine, Idaho, in the Boise National Forest, but administered by the Payette National Forest. The area surrounding the Project has been mined since the late nineteenth century by several different companies. Because of this mining legacy, the EFSFSR presently flows through the open YPP, forming a pit lake in the pit bottom, below a steep section of stream where the EFSFSR flows over the abandoned highwall. The existing YPP lake has an estimated maximum depth of 35 feet and a volume of 92 acre-feet (Brown and Caldwell 2017). Based on LiDAR data collected in 2009, the stream reach immediately upstream of the YPP has a 27% slope for at least 230 feet, reducing to 13% for the next 220 feet. These conditions are impassable for even the strongest salmonids (e.g., steelhead).

As noted above, the Project proposes to design a tunnel that will adequately convey water around the YPP for up to 12 years following mine commissioning to provide water diversion and fish passage around the YPP during future mining operations. Typical fish passage is designed to operate successfully within a narrow range of flows that have been diverted specifically for the passage component. For this Project, the design will need to account for the full range of EFSFSR flows between 95% and 5% exceedance during the respective migration periods for Chinook salmon, bull trout, steelhead, and potentially westslope cutthroat trout.

Diverting flows of the EFSFSR into a tunnel will require a diversion structure to re-route flows of the EFSFSR from its normal path. This diversion is expected to be located several hundred feet upstream of the upstream tunnel portal. Between the diversion and the upstream tunnel portal, an excavated approach channel is anticipated that will transition the river from its historical channel to the tunnel portal at the base of the hillside. The approach channel would have a low gradient to allow large-diameter bedload to fall out prior to reaching the tunnel portal. A debris rack is also anticipated as part of the design and would be located upstream of the upstream tunnel portal within the approach channel. The debris rack would exclude large woody debris and sediment larger than cobble size from the tunnel. An area for debris and sediment accumulation would be provided near the debris rack that could be accessed by tunnel maintenance equipment and personnel to clear out debris as part of routine maintenance.

The tunnel would be designed to convey the at least 500-year flow of the EFSFSR, which is approximately 721 cfs at the anticipated downstream tunnel portal location. The tunnel is also expected to provide vehicular access along the entire length of the tunnel for routine maintenance. Vehicular access would allow access to for routine cleanout; access to lighting, conduit, and structural features such as tunnel supports; and fish passage feature repair. To accommodate vehicular access, promote sediment passage, and accommodate the 500-year flow with a freeboard allowance of approximately 20% of the tunnel height, the tunnel section will be 15 feet high by 15 feet wide and D-shaped. This shape and size will provide sufficient space between the 500-year water surface elevation and the crown of the tunnel to allow for any lighting fixtures incorporated into the design.

As part of the site-wide water management plan, Perpetua plans to construct a contact water pond (Midnight Pond) upstream of the YPP with a booster tank from which water will be pumped for either water treatment and discharge or use in the process plant. In times of site-wide water deficit, Perpetua intends to supplement the site water balance with as much as 4.5 cfs of raw water from the EFSFSR. This

raw water is to be supplied by a new intake and pipeline from the EFSFSR to the booster tank, and would consist of the following elements: (1) an approved National Marine Fisheries Service (NMFS) compliant fish screen and intake, (2) a small wet well and pump house that will house the pumps, valves, controls, and other appurtenances, and (3) a pipeline extending up the adjacent hillside to the proposed location of the booster tank. The intake and screens would be situated at the tunnel headworks, upstream of the control weir.

Because of the possibility of flow depletions in the EFSFSR as a result of both pit dewatering and surface and groundwater withdrawals for process makeup water during low flow periods, the low fish passage design flow could be reduced from the current 95% exceedance flow of 8.2 cfs. For this reason, it is of interest to determine the minimum flow rate that the fishway can accommodate while meeting fish passage design criteria.

1.2.1 Task Purpose

The purpose of this task is to provide supplemental hydraulic modeling of the tunnel fishway and to investigate the lowest possible tunnel fishway flow that satisfies established fish passage design criteria by modifying the fishway weir geometry. Specifically, the analysis determines the lowest possible inflows that meet threshold flow depth and velocity criteria by way of iterative hydraulic modeling.

To this end, the following TM presents simple hydraulic calculations used to develop an approximate range of inflow boundary conditions to the CFD model, the CFD modeling setup and approach, and CFD model optimization and results.

1.3 Summary of Design Criteria

McMillen Jacobs Associates (2017; 2018) developed several design criteria related to fish passage, a subset of which is presented in Table 1 and is pertinent to this task.

Because the interest of this analysis is on determining the minimum flow through the fishway that can still meet the design criteria identified in NMFS (2022) and McMillen Jacobs Associates (2018), adjusting the fishway weir width to reduce the overall flow area over the weir would be one method of investigation. Although NMFS (2022) does not provide explicit criteria for pool-and-weir fishway weir lengths, a minimum width of 15 inches is presented for orifices, based on Bell (1991). This minimum width is considered adequate to accommodate large-bodied salmonids such as Chinook salmon and provides slightly more horizontal space for passage than does the 10-inch criterion for bar spacing of coarse trash racks in the presence of Chinook (NMFS 2022). For these reasons, a minimum weir length of 15 inches is assumed.

Table 1. Design Criteria to be Reviewed

Criteria	Value	Reference
Minimum Flow Depth	1 ft	McMillen Jacobs Associates (2018)
Maximum Flow Velocity over Weir – Bull Trout Burst Speed	6.6 ft/s	McMillen Jacobs Associates (2018)
Maximum Flow Velocity over Weir – Chinook Salmon Burst Speed	22 ft/s	McMillen Jacobs Associates (2018)
Maximum Hydraulic Drop between Fish Ladder Pools	12 in.	NMFS (2011)
Minimum weir length	15 in.	See text above.

2.0 Hydraulic Calculations

Hydraulic calculations were developed to identify a flow range for CFD simulations. Because the CFD exercise was designed to be iterative, it was of interest to reduce the “computational expense” of the modeling effort by identifying this range first using hand calculations. As an additional benefit, these calculations also serve to cross-validate model results.

2.1 Assumptions

Hydraulic calculations were predicated on the following assumptions:

1. Flow over the upstream control weir is not considered because the crest elevation of the 5-foot control weir is higher than the water surface upstream of the first fishway weir at a 1-foot flow depth over the weir and therefore the upstream control weir is not activated over the range of flows considered in this analysis. The control weir is activated at approximately 25 cfs approach flow – considerably greater than the baseflow conditions analyzed herein, with or without depletions.
2. The energy loss over the fishway weir is small and can be ignored.
3. The depth over the weir is estimated as the average of the upstream and downstream heads. The value is used for the evaluation of flow depth design criteria.

2.2 Calculation Method

The fishway weir is a submerged weir, with the submerged weir flow theoretically calculated as the difference between the free-flow discharges due to upstream and downstream heads (Villemonthe, 1947). The flow can also be approximated with the upstream and downstream head using experimental results (Villemonthe, 1947; Fox and McDonald, 1994). The weir flow and head can be calculated by comparing both flow values. Consequently, the overall procedure for the hydraulic calculation can be derived as shown in Figure 1. At first, the upstream head is assumed, then the downstream head is calculated with the required flow depth. Secondly, free-flow discharges from both heads are calculated, and then the theoretical weir flow is computed as the difference between the free-flow discharges. Thirdly, experimental weir flow is computed, assuming the hydraulic loss can be ignored. Lastly, the upstream

head is repeatedly adjusted to minimize the difference between both calculated weir flows. For the upstream head adjustment, the “solver” function in Excel is used in this calculation. Detailed equations and input parameters are discussed in the next section.

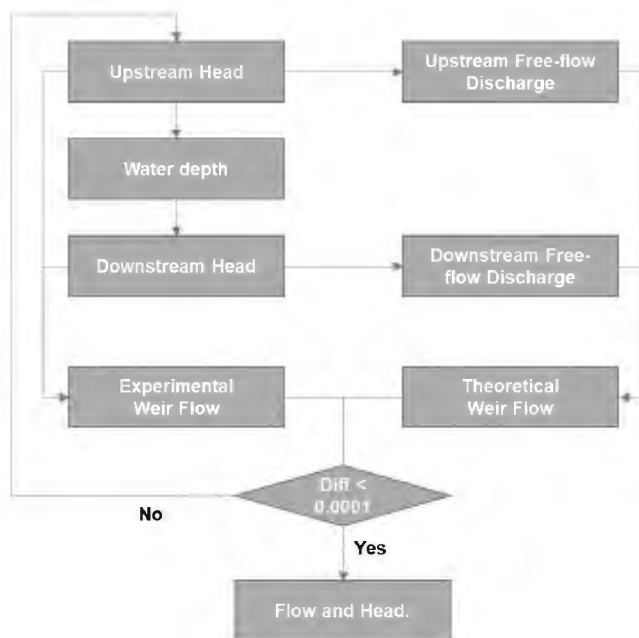


Figure 1. Hydraulic Calculation Procedure

2.3 Hydraulic Calculation

2.3.1 Input Variables

Figure 2 shows the definition of several hydraulic and geometric variables. Upstream head (H_1) and downstream head (H_2) are both measured from the channel bottom. The weir crest height (z_w) from the channel bottom is fixed at 2 ft, and the minimum flow depth over the crest is 1 ft, satisfying design criteria. Finally, the minimum weir flow height is 3 ft by adding the minimum flow depth to the weir crest height.

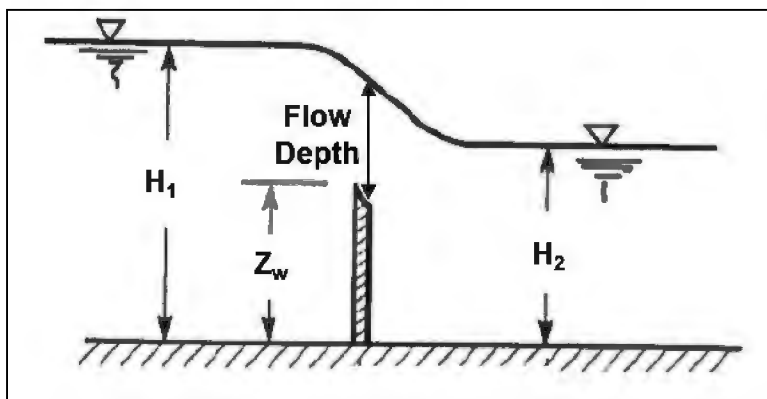


Figure 2. Schematic of a submerged weir flow

2.3.2 Hydraulic Equation

For the free-flow discharge due to hydraulic head, the following equation is used (Fox and McDonald, 1994):

$$Q_f = C_d L \sqrt{g} (H - z_w)^{3/2} \quad (1)$$

where, Q_f = free-flow discharge, [ft³/s]
 C_d = discharge coefficient
 L = weir width, [ft]
 g = gravitational acceleration (32.17 ft/s²)
 H = hydraulic head, [ft]
 z_w = weir crest height (2 ft)

The discharge coefficient is mainly affected by geometry and can be approximated using (Fox and McDonald, 1994):

$$C_d = 0.59 + 0.08 \left(\frac{H}{z_w} - 1 \right) \quad (2)$$

As a reasonable first guess, the upstream head (H_1) is assumed to equal 3.500 ft. Because the downstream head (H_2) is equidistant from the weir flow elevation, and the weir flow elevation is assumed to be 1 ft above the weir crest (i.e., 3 ft above the channel bottom), the downstream head is calculated as 2.500 ft, and the free-flow discharges upstream and downstream are determined initially as shown in Table 2.

Table 2. Calculation example on upstream and downstream free-flow discharge

	H [ft]	Z _w [ft]	C _d	H-z _w [ft]	L [ft]	Q _f [ft ³ /s]
Upstream	3.500	2	0.650	1.500	1.25	8.466
Downstream	2.500	2	0.610	0.500	1.25	1.529

Therefore, as the difference between the upstream and downstream free-flow discharges, the theoretical flow over the submerged weir is calculated as 6.937 ft³/s.

The weir flow can also be determined based on the experimental relationship of the head ratio over the crest, according to (Villemonste, 1947):

$$Q_w = Q_f \left(1 - \left(\frac{H_2 - z_w}{H_1 - z_w} \right)^n \right)^m \quad (3)$$

where, Q_w = weir flow over the submerged weir, [ft³/s]
 n, m = exponents

Typically, m equals 0.385, and for a rectangular contracted weir, the exponent n is 1.45 (Villemonthe, 1947). Although the weirs in the proposed fishway are only contracted on one side, these values are nevertheless adopted for simplicity. Assuming that energy loss can be ignored, the weir flow can be determined approximately as:

$$Q_w \approx Q_f \left(1 - \left(\frac{H_2}{H_1} \right)^{1.45} \right)^{0.385} \quad (4)$$

Based on this equation and the initial assumptions above, the weir flow is approximately 5.869 ft³/s.

Using these methods, the upstream head is determined by iteratively adjusting its value so that the weir flow in Eq. (4) is the same as the weir flow calculated from Table 2. Going through this exercise, the resulting upstream head is 3.255 ft, and the weir flow is 3.556 ft³/s.

2.3.3 Results and Simulation Cases

As demonstrated above, when flow depth is 1 ft, the upstream head and weir flow are expected to be 3.255 ft and 3.556 ft³/s, respectively. The average velocity over the weir is estimated as 2.84 ft/s. This satisfies the design criteria of Table 1. In this equation, the hydraulic drop (the subtraction of the downstream head from the upstream head) is 0.5 ft, which is substantially larger than zero, suggesting that the actual flow rate might be more than calculated in the spreadsheet. Therefore, CFD simulation flows were derived by multiplying the previously-calculated flow rates by a scaling factor. Scaling factors were developed using judgment in an attempt to bound the results that would be reflected in the CFD model. The scaling factors range from 1.40 to 2.25, and the simulation flows range from 5.0 ft³/s to 8.0 ft³/s. Consequently, the cases shown in Table 3 were simulated in CFD and evaluated against the minimum flow depth design criterion. The flow rates are used for CFD model inflow boundary conditions in each case.

Table 3. Simulation cases for 1-foot flow depth

Simulation Cases	Case 1	Case 2	Case 3	Case 4
Scaling Factor	1.40	1.85	2.00	2.25
Volumetric Flow Rates, [ft ³ /s]	5.0	6.6	7.1	8.0

Additionally, flow at 2 feet of depth was also calculated to determine the maximum flow rate over the weir beyond which the upper portion of the weir wall would be overtopped. Overtopping of the upper portion of the weir wall is not ideal from a fish passage perspective because it could falsely attract fish to pass over that portion of the weir, which is inherently more difficult, rather than attempting to pass over the weir notch, which is much more passable by design. This upper flow limit was calculated to be 16.1 ft³/s. Applying scaling factors ranging from 0.90 to 1.55, simulation flow rates ranged from 14.5 ft³/s to 25.0 ft³/s for the cases shown in Table 4.

Table 4. Simulation cases for 2-foot flow depth

Simulation Cases	Case 5	Case 6	Case 7	Case 8
Scaling Factor	0.90	1.00	1.25	1.55
Volumetric Flow Rates, [ft ³ /s]	14.5	16.1	20.2	25.0

3.0 Hydraulic Modeling

3.1 Model Development

The commercial software, FLOW-3D by Flow Science, Inc, was used for the fish passage modeling. The software solves the Navier-Stokes equations of fluid flow in three dimensions. It is widely used for analyzing open channel flow on water resources projects. The simulation results are solved and evaluated in a quasi-steady state. Less than 1 percent variation from the mean indicates that the simulation is nearly steady state. Post-simulation work for analyzing the results was performed using FLOW-3D POST 1.1.0. All simulations were solved with 16 cores in a Microsoft workstation (Operating system: Windows Server 2019, Memory: 128 GB, CPU: Intel Xeon 2.20 GHz). Details on model setup are discussed in the sections below.

3.1.1 Assumptions

The CFD model setup includes the following assumptions:

1. Isothermal conditions are used. Even though the effect will be very minor, heat can nevertheless affect the viscosity of flow.
2. The flow over the weir is affected by the adjacent upstream and downstream fishway pool. Because the model only includes three weirs, the interior weir was adopted as the representative weir because it is unaffected by upstream and downstream boundary conditions.
3. The hydraulic modeling ignores any materials entrained in the flow path such as debris or sediment. The modeling simulates low-flow conditions during which little or no debris or sediment is transported; in addition, control measures are in place upstream for capturing debris and sediment. Therefore, this is expected to be a reasonable assumption.

3.1.2 Governing Equations

The volume-averaged conservation of mass and momentum in steady state are given by the following equations, respectively:

$$\nabla \cdot (\rho V) = 0 \quad (5)$$

$$\nabla \cdot (\rho VV) = -\nabla p + \nabla \cdot (\mu \nabla V) + \rho g \quad (6)$$

where, ρ = density [lb/ft³]
 V = velocity [ft/s]
 μ = viscosity [lb s/ft²]
 p = pressure [lb/ft²]

The Renormalized Group (RNG) model was used for solving turbulence closure, which is widely accepted for open channel water flow problems.

3.1.3 Geometry and Mesh

The simulation domain and geometry are shown in Figure 3. The geometry of the simulated area is 120 x 40 x 9.5 ft, presenting a part of the upstream end of the fishway. It includes the 4-foot-tall control weir, a 5-foot-tall divider wall, and three fishway weirs. The distance between the adjacent fishway weirs is 22 ft. The 1st and 3rd weirs are affected by inflow and outflow boundary conditions, respectively. The 2nd weir is chosen for the detailed analysis of simulation results. The fishway weir crest is 2 ft from the channel bottom, and its width is 1.25 ft (15 inches). The width was established initially as 2 ft (McMillen Jacobs Associates, 2018), but is modified here to help identify the lowest possible fishway flow that still meets the fish passage design criteria (see discussion in Section 1.3). The width of the fishway and accessway are 5 ft and 9 ft, respectively. The thickness of the divider wall is 1 ft. Thus, the overall width of the EFSSFR tunnel is 15 ft. The longitudinal slope of the tunnel accessway and fishway is 4.5%.

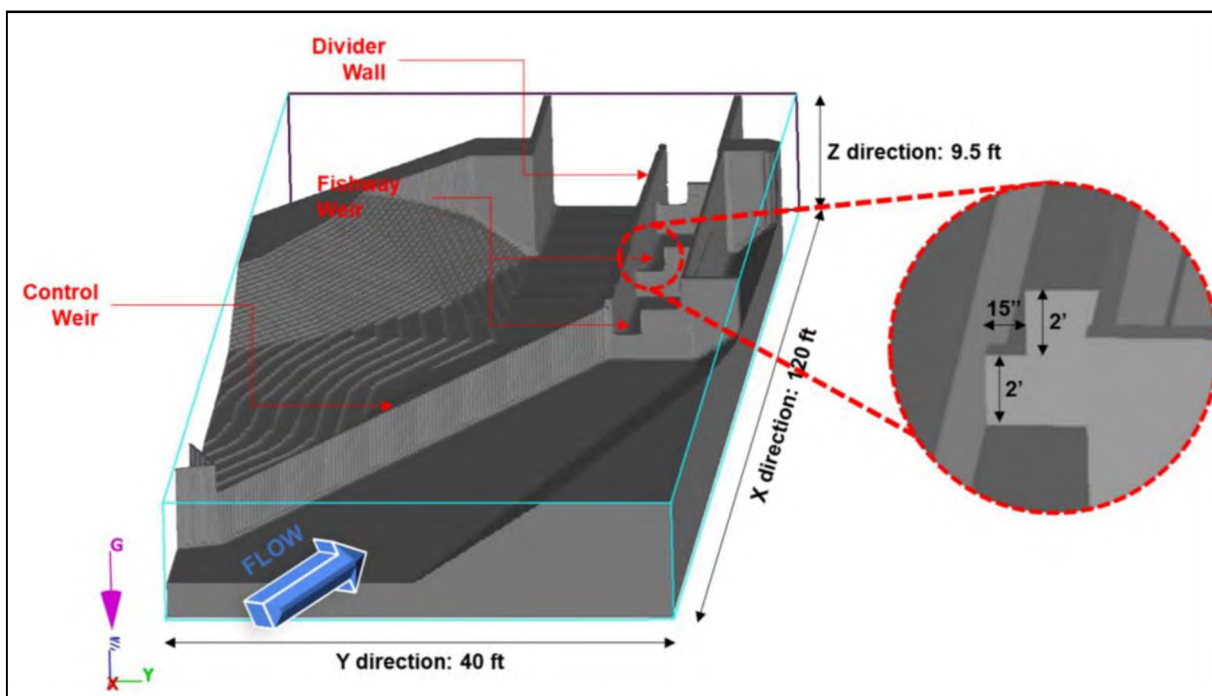


Figure 3. Simulation Domain and Geometry

3.1.4 Initial and Boundary Conditions

The initial water surface elevation is 61.5 ft, which is referenced to an arbitrary model-only datum. All computed fluid regions are submerged to some extent, but all water is discharged through outflow boundaries. The closer the initial condition to the steady state results, the shorter the overall simulation time. The simulation boundary conditions specify a user-specified volumetric flow rate at the upstream end and an outflow boundary condition at the downstream end of the domain. Symmetry boundary conditions are applied to other boundaries. The flow rate boundary condition uses a fluid elevation of 60.5 ft to initially approximate the 1 foot of flow depth over the weirs. The symmetry boundary condition is subject to a zero-gradient condition at the boundary and a zero-velocity condition normal to the boundary (Flow Science, 2015).

Roughness is applied at the solid boundary. The roughness in FLOW-3D is simulated with roughness height (Flow Science, 2015). A roughness height of 0.001 ft is used for the concrete surface.

3.2 Results and Discussion

3.2.1 Mesh Adjustment

Typically, fine meshing leads to accurate simulation results. However, it also incurs a high “computational expense” due to the associated small timestep size and resulting large number of solutions required. Cell size was therefore investigated to determine the optimum cell size for widescale simulation. Results are shown in Table 5 along with associated simulation runtimes and results.

Table 5. Model cell size vs. model performance.

Cell size [ft]	Numbers of Cells	Runtime [hrs]	Flow Depth [ft]
0.350	1,055,754	6.1	0.54
0.300	1,702,400	6.1	0.72
0.275	2,212,700	16.5	0.74
0.250	2,918,400	25.3	0.72

Table 5 shows the simulation cases that were run to define the optimal mesh size. The simulation was run with a 5 ft³/sec inflow condition. From the table, as cell size decreases from 0.350 ft to 0.250 ft, the number of cells increases by approximately 2.9 times from 1 million to 2.9 million. Runtime is also significantly increased by more than three times. At a cell size of 0.350 ft, it takes about 6 hours, while over 25 hours are needed using a cell size of 0.250 ft. The flow depth can be obtained from point data in the cross-section flow over the weir crest. Figure 4 shows the relationship between the number of cells/runtime and the flow depth. In Figure 4, the abscissa presents flow depth over the 2nd weir crest, and the left ordinate and right ordinate denote the number of cells and runtime, respectively. As previously mentioned, fine meshing can lead to more accurate results, but runtimes are significantly increased. As shown in Table 5 and Figure 4, the model error gradually decreases with decreasing cell size, with decreases in model error tapering off sharply as the mesh cell size approaches 0.300 ft. Therefore, a cell size of 0.300 ft was determined to be optimal for running the various models to acquire flow depth over the weir, considering computational load and accuracy of simulation results.

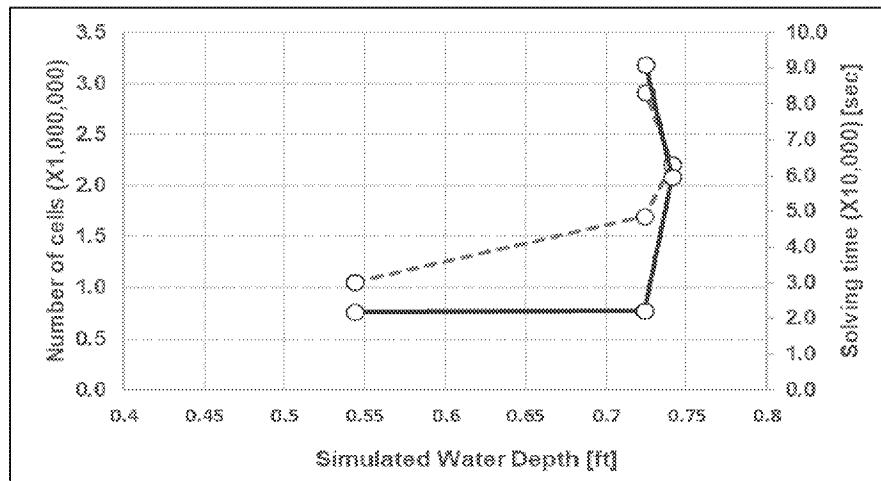


Figure 4. Simulation results with cell numbers and solving time

3.2.2 Simulation Cases

The following section presents the CFD simulation case results for both 1 foot and 2 feet of depth over the fishway weir. The section provides results for water depth over the weirs, associated flow rates, and average cross-sectional velocities over the weirs.

3.2.2.1 1-foot Flow Depth

The point data in each cell is used to determine the 1-foot flow depth. The points are limited to the cross-section in the middle of the 2nd weir. The 1-foot flow depth is derived by subtracting the weir crest elevation from the free surface elevation. The point data were also evaluated against other design criteria, such as velocity over the weir and hydraulic drop between pools. Table 6 shows the simulation results to determine the flow rate for 1-foot flow depth over the weir.

Table 6. Results for Cases 1 through 4.

Case	Flow Rate [cfs]	Weir Depth [ft]
1	5.0	0.72
2	6.6	0.92
3	7.1	0.99
4	8.0	1.08

The values presented in Table 6 result in the following linear regression line:

$$\text{Flow Depth [ft]} = 0.1213 \times \text{Flow Rate [ft}^3/\text{s]} + 0.1206 \quad (7)$$

This regression line has a p-value much less than 0.05 and a coefficient of determination (R^2) of 0.997. Therefore, the relationship shown in Equation 7 is considered statistically significant and reliable for estimating the flow depth. The 1-foot flow depth calculated by this curve occurs at 7.25 ft³/s, and ranges from 6.89 to 7.61 ft³/s considering a $\pm 5\%$ confidence level, as shown in Figure 5.

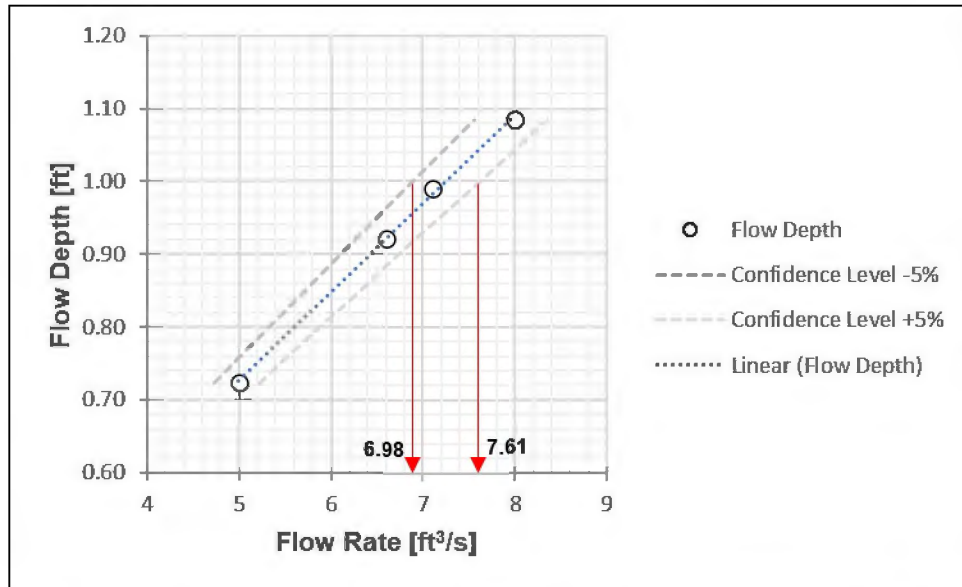


Figure 5. Case study results for estimating the flow rate corresponding to 1 foot depth

The simulated velocities over the weir are presented in Table 7, along with associated standard deviations. Although the velocities vary, the average velocity is less than the maximum design criterion of 6.6 ft/s.

Table 7. Velocity over the weir in 1-foot depth cases

	Case 1	Case 2	Case 3	Case 4
Volumetric Flow Rate [ft³/s]	5.0	6.6	7.1	8.0
Average velocity [ft/s]	5.80	6.13	6.10	6.20
Standard deviation [ft/s]	0.58	0.64	0.63	0.62

For calculating the hydraulic drop between pools, upstream and downstream cross-section data are used. The upstream and downstream cross sections are located 10 ft from the weir in the upstream and downstream directions. As depicted in Figure 6, both upstream and downstream heads increase with flow rates, but the hydraulic drop between pools is nearly uniform at 0.66 ft in all cases. Because the hydraulic drop between pools is less than the design criterion of 1.0 ft in all cases, each case satisfies the design requirement for hydraulic drop. **Consequently, 7.25 ft³/s of volumetric flow rate will meet the minimum flow depth of 1 ft as well as the other design criteria such as velocity and hydraulic drop. Lower flow rates will meet velocity and hydraulic drop criteria, but will have less than 1 foot of depth over the weir.**

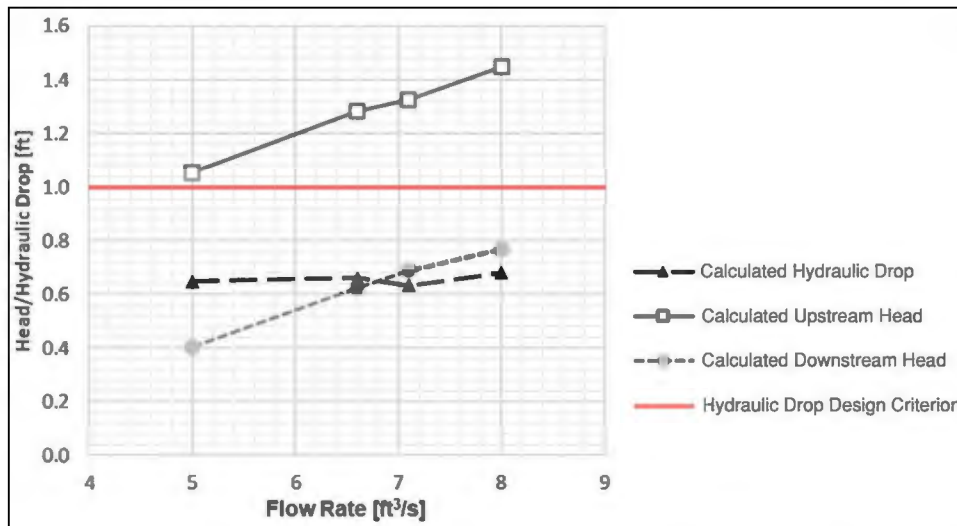


Figure 6. The hydraulic drop between pools in Case 1 to Case 4 (1-ft depth scenario)

3.2.2.2 2-foot Flow Depth

This section presents the results in Case 5 through Case 8 to determine the volumetric flow rate for 2 feet of flow depth over the weir. The calculation of the flow depth utilizes point data in the cross-section, as explained in the previous section. To prevent overflow from the upstream control weir, the modeled control weir crest height artificially increases for the high flow rates. As shown in Figure 7, each point presents simulation results between flow rates and flow depth in the 2nd weir. To determine the flow rate for 2-foot flow depth, a linear regression was performed as in the previous case analysis. The linear regression is derived as

$$Flow\ Depth\ [ft] = 0.0359 \times Flow\ Rate[ft^3/s] + 1.319 \tag{8}$$

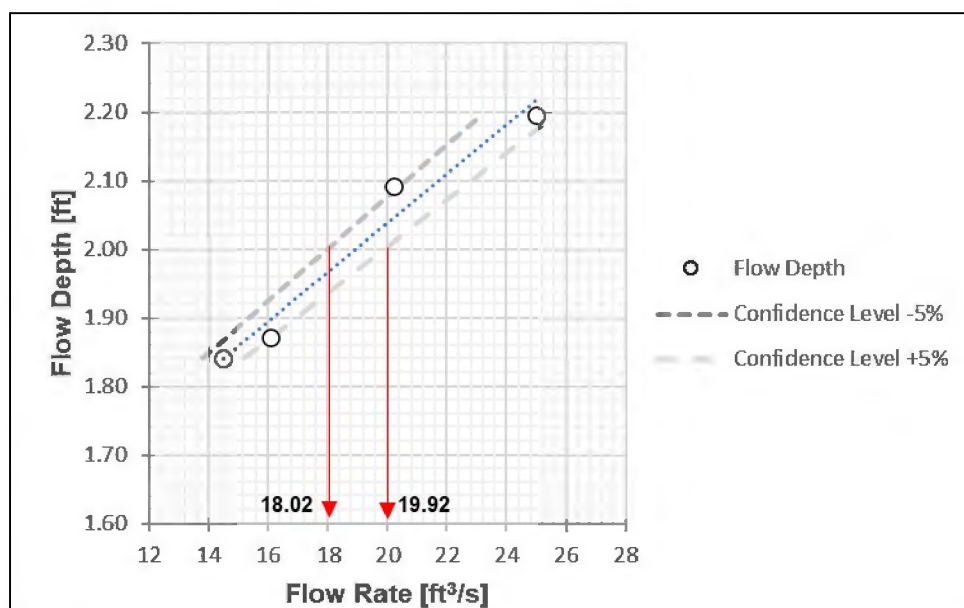


Figure 7. Case study results for estimating the flow rate corresponding to a 2-foot depth

The regression curve has a p-value of 0.019 and a coefficient of determination greater than 0.96. Thus, the curve is statistically significant and reliable. Eq. (8) results in a flow rate of 18.97 ft³/s for 2 feet of depth. Applying a ±5% confidence level, the flow rate is between 18.02 and 19.92 ft³/s, as depicted in Figure 7.

The average velocities for Case 7 and Case 8 are over 6.6 ft/s, as reported in Table 8. However, the average velocity is derived from the flow over the submerged weir in those cases, which is higher than the anticipated threshold flow rate of 18.97 ft³/s. For this reason, weir flows at 2 feet of depth are expected to have associated velocities at or below 6.6 ft/s.

Table 8. Velocity over the weir in 2-foot depth cases

	Case 5	Case 6	Case 7	Case 8
Volumetric Flow Rate [ft ³ /s]	14.5	16.1	20.2	25.0
Average velocity [ft/s]	6.28	6.30	6.69	7.29
Standard deviation [ft/s]	1.44	1.22	0.89	1.08

The hydraulic drop between fishway pools for Cases 5 through 8 is greater than in the 1-foot depth cases, as shown in Figure 8. Nevertheless, the maximum hydraulic drop is still less than the 1-foot design criterion. **Consequently, the hydraulic simulations presented above show that the flow rate over the weir at 2 feet of depth is 18.97 ft³/s and that this flow rate meets the pertinent design criteria for depth, hydraulic drop and velocity.** The control weir will therefore have a crest elevation set to pass the remainder of the 5% exceedance flow (54.00 cfs – 18.97 cfs = 35.03 cfs). This is expected to be approximately 0.3 feet below the contracted fishway weir, leaving approximately 1.7 feet of vertical space over the fishway weir for river flows below the 5% exceedance flow. In other words, at the low fish passage design flow water will not be split between the fishway and the control weir.

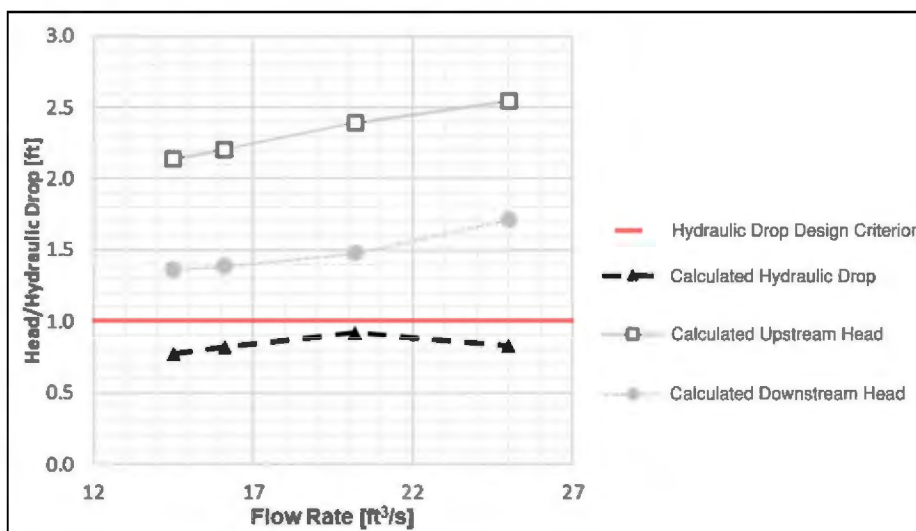


Figure 8. Hydraulic drop between pools in Cases 5 through 8 (2-ft depth scenario)

4.0 Summary and Conclusions

The hydraulic modeling described in this TM was developed to determine the volumetric flow rates that lead to a 1- and 2-foot flow depth over the fishway weir in the EFSFSR Tunnel. These flow depths are of interest because a 1-foot depth meets an important fish passage criterion for minimum depth at the low fish passage design flow (95% exceedance flow) and a 2-foot depth corresponds with the outer wall height of the weir and the high fish passage design flow (5% exceedance flow). These two flow depths therefore capture the range of fish passage design flows for the facility. A variety of inflow rates were used as boundary conditions to a CFD model of the fishway. The inflow rates were determined by a spreadsheet model to develop a finite set of cases that would allow the modeler to identify flow rates corresponding with 1 foot and 2 feet of weir flow depth at a lower computational cost.

Hydraulic calculations using the spreadsheet model estimated flow rates of 3.5 ft³/s for 1 foot of weir flow depth and 16.1 ft³/s for 2 feet of weir flow depth. Several scaling factors were determined using engineering judgment to arrive at a series of cases with different flow rates to help minimize the number of iterations required for CFD model simulation. The resulting flow ranges for CFD modeling were 5.0 ft³/s to 8.0 ft³/s for the 1-foot depth, and 14.5 to 25.0 ft³/s for 2-foot flow depth.

Prior to commencing with CFD simulation, the cell size was reviewed in order to identify the optimal cell size in terms of model accuracy and computational efficiency. Results indicate that a 0.3-foot cell size is optimal.

Results of the CFD simulations indicate that a flow rate of 7.25 ft³/s (6.89 to 7.61 ft³/s, ±5% confidence level) is required to achieve a 1-foot weir flow depth over a 15-inch-wide weir; lower flows will result in flow depths not meeting the 1-foot criterion. Results also indicate that a flow rate of 18.97 ft³/s (18.02 to 19.92 ft³/s, ±5% confidence level) is required to achieve a 2-foot weir flow depth. In both of these cases, the average velocity over the weir is expected to be less than 6.6 ft/s, which satisfies fish passage criteria for maximum velocity.

For smaller non-anadromous species such as Cutthroat trout, the flow depth criterion will be lower. Although passage criteria for these species do not govern the overall design, it is of interest to Project stakeholders what the lower limits of passability through the fishway for these and other species might be. To this end, the results presented above for the lowest flow case (Case 1) may be instructive, whereby a total fishway flow of only 5 cfs leads to a weir flow depth of 0.72 feet, an average velocity of approximately 5.8 ft/s, and a hydraulic drop from pool to pool of approximately 0.64 feet.

5.0 References

Brown and Caldwell, 2017. Stibnite Gold Project Water Resources Summary Report, prepared for Midas Gold Inc., Valley County, Idaho, June 30, 2017.

Flow Science (2015). FLOW-3D Version 11.1 User's Manual.

Fox, R.W., and McDonald, A.T. (1994). Introduction to Fluid Mechanics 4th Ed. New York: John Wiley & Sons.

McMillen Jacobs Associates (2017). Technical Memorandum No. 01: EFSFSR Fish Passage Design Guidance Criteria and Preliminary Alternatives Analysis.

McMillen Jacobs Associates (2018). Midas Gold Idaho, Inc. Stibnite Gold Project Feasibility Study - East Fork South Fork Salmon River (EFSFSR) Tunnel Design Documentation Report.

McMillen Jacobs Associates (2019). Technical Memorandum No. 11: EFSFSR Fish Passage Tunnel – Accessway and Fishway Hydraulics.

NMFS – National Marine Fisheries Service (2011). Anadromous Salmonid Passage Facility Design. July 2011.

Villemonte, J.R. (1947). Submerged-Weir Discharge Studies. Engineering News-Record. 139(26). 54-46.

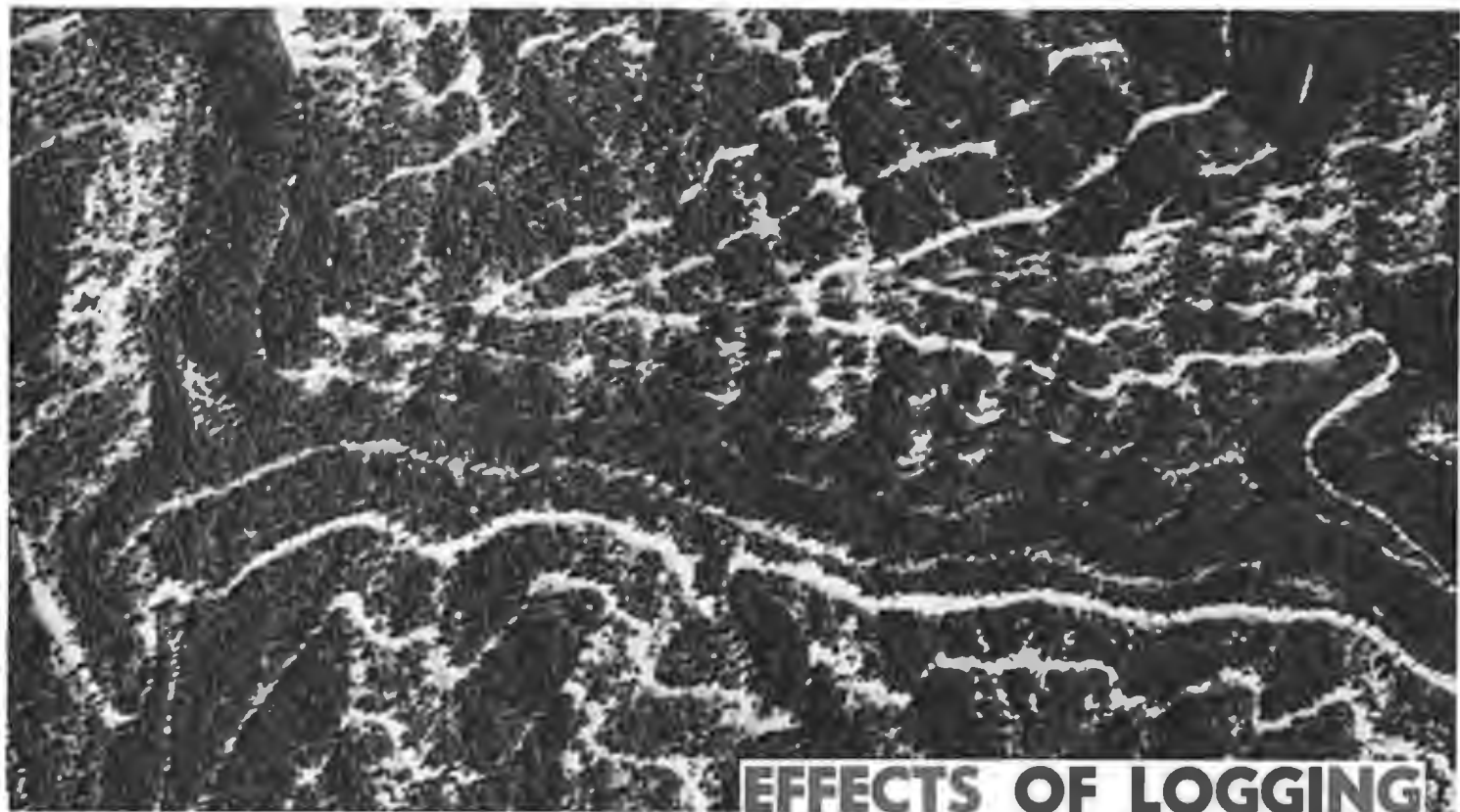


Fig. 1. Aerial view of the road network in a jammer logging operation during the period 1955 to 1959 in the Cow Creek drainage, Payette National Forest, Idaho. Between 25 to 30 percent of this area was bared by road construction.

EFFECTS OF LOGGING AND LOGGING ROADS ON EROSION AND SEDIMENT DEPOSITION FROM STEEP TERRAIN

ABSTRACT—Erosion plots and sediment dams were used to evaluate the effects of jammer and skyline logging systems on erosion and sedimentation in steep, ephemeral drainages in the Idaho Batholith of central Idaho. Five-year plot data indicated that no difference in erosion resulted from the two skidding systems as applied in the study. Sediment dam data obtained concurrently showed that the logging operations alone (excluding roads) increased sediment production by a factor of about 0.6 over the natural sedimentation rate. Roads associated with the jammer logging system increased sediment production an average of about 750 times over the natural rate for the six-year period following construction.

The more accessible timbered areas in the southern part of the Idaho Batholith in south-central Idaho were logged, using either tractor or jammer-skidding meth-

ods, during the 1940's and 1950's. Soil disturbance, erosion and subsequent downstream sediment damage from these methods were minimal, primarily because logging was confined to areas of subdued topography (4). However, when logging was begun on areas of steeper topography, these methods became undesirable because tractor skidding was hazardous on slopes where gradients exceeded 50 percent, and jammer skidding required a dense network of roads. Some of these jammer-logging operations on steeper slopes disturbed 25 percent or more of the area by construction alone (Fig. 1).

In 1955, the Brown Tie and Lumber Company, using a mobile spar, did the first skyline logging in the Idaho Batholith. Although the new method was not entirely satisfactory, it was encouraging because logs could be skidded more than twice as far as when using a jammer; thus, only about half as much road construction was required. In addition, soil disturbance and

damage to the residual stand were minimized because the logs were often partially or completely suspended for most of the distance from the stump to the landing.

Initial results of skyline logging showed enough promise to warrant additional study. In 1959 the Zena Creek Logging Study was established on about 15,000 acres of steep mountain lands in south-central Idaho. This joint venture included: (a) a timber sale using mobile spar and radio controlled sky car equipment (skyline), conventional jammer and tractor skidding methods; (b) an administrative study to inventory resource values and evaluate costs and effects of timber sale operations and treatments; and (c) research on impacts of logging on watershed values, tree planting success, time-cost evaluations of log yarding and loading and road engineering (3).

This study was a major part of the watershed management research program designed to compare the effects of jammer vs. skyline logging systems with respect to on-site erosion and subsequent sediment movement into ephemeral stream channels. Its justification was based on indications that logging and attendant road construction in the vicinity were damaging the fishery resources of the South Fork of the Salmon River, especially the anadromous fish (5).

Description of the Study Area

The study area (Fig. 2) is located near the confluence of the Secesh River and the South Fork of the Salmon River in the south-central portion of the 16,000-square-mile Idaho Batholith. It is near the head of the Deep Creek drainage at an elevation of about 5,000 feet mean sea level. The sandy loam to loamy sand soils average about 16 inches deep and exhibit little or no B-horizon development. They are formed from acidic, intrusive bedrock; quartz monzonite is dominant. Annual precipitation averages 28.3 inches. About 60 percent occurs during the colder months as snowfall, 15 percent as rain during the period from June through

W. F. Megahan

W. J. Kidd



Megahan is principal forest hydrologist, Intmntn. Forest and Range Exp. Sta., Ogden, Utah, stationed at Forestry Sci. Lab., Boise, Idaho; Kidd was formerly at the Forestry Sci. Lab., Boise, and is now with the NE Area, State and Private Forestry, Columbus, Ohio.

Table 1. Average Erosion from Plots on the Jammer and Skyline Logging Units.

Measurement period	Jammer unit		Skyline unit	
	Mean erosion	Number of plots ¹	Mean erosion	Number of plots ¹
	Tons/sq mile		Tons/sq mile	
9/61-5/62 ²	—	8	—	8
5/62-9/62	5.8	4	25.1	7
9/62-5/63 ²	6.1	5	18.6	8
5/63-9/63	7.8	5	17.3	8
9/63-5/64	5.3	5	17.7	8
5/64-9/64	32.4	5	21.2	8
9/64-5/65	9.8	4	43.6	5
5/65-9/65	22.2	3	46.1	7
9/65-5/66	2.8	5	30.9	8
5/66-10/66	8.0	5	32.8	8
10/66-5/67	2.4	5	21.0	8
5/67-9/67	1.3	4	0.3	7

¹ Two plots were obliterated by road construction; one by logging on the jammer unit. In some instances, plot data were rejected because of such accidental errors as trampling by deer and elk, effects of ground squirrels, etc.

² Jammer roads built in October 1961.

³ Both units logged during October and November 1962.

August, and the remainder during the spring and fall. Slopes are steep, averaging 67 percent, with the dominant aspect west grading to northwest and southwest on finger ridges. Prelogging volumes of commercial timber totaled 12,560 bd. ft/acre on the jammer unit and 11,210 bd. ft/acre on the skyline unit, consisting of about 75 percent ponderosa pine and the remainder Douglas-fir.

Study Design

The average width of Deep Creek study area was 550 ft. extending from the drainage divide to a lower-lying main log-haul road (Fig. 3). The long axis of the area was about 3,200 ft. and bisected the top of numerous small, ephemeral drainages. The area was divided into two cutting units of 21.5 and 22.4 acres, where jammer and skyline logging systems, respectively, would be applied.

The study was designed to compare on-site erosion and subsequent movement of sediment that was the result of the above two logging systems in the ephemeral stream channels. Installations consisted of eight 1/100-acre erosion plots with wooden borders and catch troughs in each cutting unit, and eight sediment dams in ephemeral drainages. Five dams were in the skyline unit and three in the jammer unit. The erosion plot data provide a comparison of the effects of the two logging systems on on-site erosion, excluding road construction. Sediment data from dams represent the effect of felling and skidding on the skyline unit and felling and skidding plus road construction on the jammer unit.

The sediment dams and erosion plots were constructed in November 1960 and September 1961, respectively. Standard construction practices were used to build the jammer roads during October 1961. During the period from October 25, 1962, to November 14, 1962, 230,000 and 214,000 bd. ft. of timber were removed from the skyline and jammer units, respectively. Standard post-logging erosion control measures were installed on the jammer roads including water bars and grass seeding.

Table 2. Average Sediment Accumulations in Dams in Ephemeral Drainages

Measurement periods	Elapsed time (days)	Jammer unit			Skyline unit		
		Average sediment caught (tons/sq. mile)	Sample		Average sediment caught (tons/sq. mile)	Sample	
			Number drainages	Total areas (acres)		Number drainages	Total area (acres)
11/60- 6/61	232	0	3	10.0	0	5	12.0
6/61- 6/62 ¹	372	5,424	3	10.0	0	5	12.0
6/62-10/62	121	402	3	10.0	0	5	12.0
10/62-11/62	21	-----	----- Period of logging on both units --no sediment measurements -----				-----
11/62- 5/63	196	440	3	10.0	4	5	12.0
5/63- 9/63	114	224	3	10.0	38	5	12.0
9/63- 5/64	252	34	3	10.0	1	5	12.0
5/64-10/64	129	0	3	10.0	5	5	12.0
10/64- 6/65	253	17,492	3 ²	10.0	13	5	12.0
6/65- 9/65	105	58	2	5.3	0	5	12.0
9/65- 6/66	259	340	2	5.3	0	5	12.0
6/66- 9/66	101	0	2	5.3	0	5	12.0
9/66- 5/67	220	61	2	5.3	0	5	12.0
5/67- 9/67	121	180	2	5.3	4	5	12.0

¹ Jammer roads constructed October 1961.

² Dam number 3 irreparably destroyed by a land slip on 4/23/65. Field measurements indicated 6,030 ft³ of material moved down the channel.



Fig. 2. General view in the vicinity of the Deep Creek study area. Note the mobile spar, skidder-loader in operation.

All material caught in the erosion plot troughs was carefully collected and dried and weighed in the laboratory. Sediment accumulations behind dams were surveyed, using standard procedures. Data from the erosion plots and sediment dams were collected twice annually on or about June 1 following the snowmelt period and near the end of the water year on or about September 30. Data collection continued on schedule

until September 1967.

Jammer Skidding vs. Skyline Skidding

The erosion plots were designed to catch soil eroded solely from within the confines of the plot border. Thus, the data eliminate the effects of road erosion or conversely provide a direct comparison of the erosion generated by the jammer and skyline skidding systems.

Statistical tests showed no significant differences in

means of the following physical characteristics of erosion plots located on the two logging units: (a) slope aspect; (b) slope gradient; (c) soil depth; and (d) the percentage of ground cover before logging (includes basal area of plants plus litter). Since all drainages studied were in a relatively small area and there were no significant differences in the above physical characteristics, it was possible to conduct statistical tests for differences in the means of erosion for plots on the jammer and skyline units. However, the standard deviations of the erosion plot data were found to be proportional to the means. A $\log_e (X + 0.5)$ transformation of erosion data was used to provide a more reliable test for differences. A test for homogeneity of variances among the 22 groups of data (two logging systems for 11 periods) confirmed the validity of the transformation (1). An analysis of variance showed no significant differences between the two logging methods with respect to on-site erosion; however, there were differences in erosion between the measurement periods (Table 1).

Usually, one would expect that skyline logging would produce less erosion than jammer logging. This is because in the skyline method the logs are usually lifted above the ground and carried part or most of the way from the stump to the landing; conversely, in the jammer system, logs are dragged over the soil surface for the entire distance.

Maximum ground clearance is attained when skyline logging is used on concave slopes. However, the slopes on the study area varied from straight to convex and thus we probably experienced more soil disturbance with the skyline system than might be expected. In addition, the logs were skidded downhill by the skyline system. This was contrary to normal operating procedures and thus the loggers found it difficult to control the descent of the logs and still maintain ground clearance. This also helped increase the soil distur-

ance and the consequent soil erosion on the skyline unit relative to that on the jammer unit.

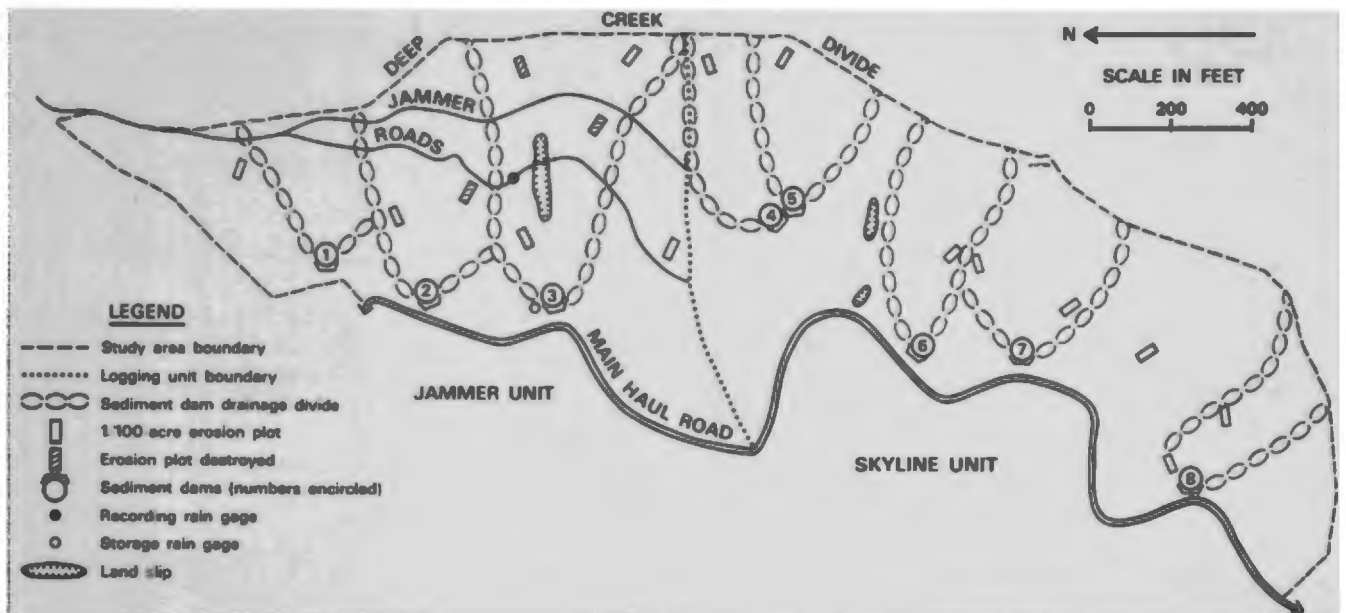
Effects of Road Construction

Data from the sediment dams on the skyline unit provide a comparison of the pre- and post-logging conditions. Sediment data from the jammer unit allow us to compare sediment production for undisturbed conditions to sediment production after road construction and also to sediment production after road construction plus logging. Finally, by comparing the two units we can isolate the effects of road construction on the jammer unit (Table 2).

Consider first the skyline unit where no measurable sediment deposits occurred during the two-year period previous to logging. Note that sediment production occurred immediately following logging and continued at a moderate rate for about 2.5 years. This was followed by a two-year period of no sediment. A small amount of sediment production occurred during the last four months of the study. Field observations showed that the sediment from the skyline unit resulted from erosion on skid trails.

The jammer unit likewise had no measurable sediment deposition in any of the sediment dams prior to road construction. Then, road construction on the jammer unit produced a great amount of sediment deposition. However, on the skyline unit, sediment continued to be too insignificant to be measured. All the sediment deposited in dams on the jammer unit during this pre-logging period resulted from erosion on roads. Sediment deposition was considerably higher on the jammer unit than on the skyline unit during the first three measurement periods following logging, again reflecting the added influence of road erosion. All road erosion up to this time had been confined to movement of individual particles within the road prisms by forces at the soil surface; this is often referred to as sheet and gully

Fig. 3. A schematic map of the Deep Creek study area.



erosion. One of the largest rain and snow storms on record for this area occurred during late December 1964. This was a rain on snow event that caused considerable landslide damage on both undisturbed and logged-over lands up to a maximum elevation of about 5,000 ft. over much of southern and central Idaho. The following April a second series of storms released 3.4 inches of rain on the melting snowpack while active snowmelt was occurring at higher elevations. This second storm caused landslide damages up to an elevation of 6,000 ft.¹ Most of the damage on logged areas was associated with roads and was often due either to improper location or construction practices such as lack of fill compaction, or both.²

Similar storm events in 1955 caused natural landslides in the study area (Fig. 3). The lower jammer road was built in October 1962 across the largest of these old slides. During the April storms of 1965 this road construction failed and resulted in a slide that produced approximately 270 tons of material (Fig. 4). The slide destroyed sediment dam number 3 and scoured the channel to bedrock, thus preventing reconstruction of the dam. Improper road location and construction practices caused this slide.

The measurement periods following the landslide revealed that sediment deposition on the jammer unit was continuing at a higher rate than on the skyline unit. Again, this reflected the impact of surface erosion on the jammer roads.

The average sedimentation rates on the two cutting units for the duration of the three test periods of: (a) no disturbance; (b) road construction; and (c) road construction-plus-logging are shown in Table 3.

Natural sediment deposition apparently was increased an average of 0.04 ton/sq. mile/day by skyline logging as compared to the undisturbed state. This is a reasonable conclusion because field observations showed that erosion was occurring on skidtrails in the unit.

The immediate effect of logging road construction is obvious. Following road construction, sediment deposition averaged 11.81 tons/sq. mile/day as compared to zero for the previous period on both units and zero for the same period on the skyline unit.

¹F. Jensen and G. Cole. The South Fork of the Salmon River storm report. Unpub. rep., Payette National Forest, McCall, Idaho. 36 p. 1965.

²R. B. Gardner, M. J. Gonsior, and G. L. Martin. Zena Creek road and logging system investigations. Unpub. rep. of the Intmtn. Forest & Range Exp. Sta. Forest Sci. Lab., Bozeman, Mont. 1968.

Table 3. Average Sediment Deposition Before and After Road Construction and Logging on the Deep Creek Study Area

Activities	Period of time sampled	Mean sediment deposition	
		Jammer	Skyline
No logging, no roads	Years		
Roads in jammer unit—no logging	0.65	0.00	0.00
Roads in jammer unit—both units logged	1.35	11.81	0.00
	4.80	10.76	0.04

Based upon the results of the erosion plot study, we can assume that the jammer and downhill skyline skidding methods caused equal amounts of erosion. Thus, we would expect an average of 0.04 ton/sq. mile/day of soil movement on the jammer unit following logging; this value subtracted from the value of 10.76 tons/sq. mile/day (shown in Table 3) gives 10.72 tons/sq. mile/day as the increase in sediment production due to road erosion after logging. The above values for road erosion apply to the total watershed area on the jammer unit. However, only a total of 2.1 acres of the total area of 10 acres sampled was actually disturbed by road construction. Since the erosion was occurring only within this 2.1 acres, the actual erosion rates due to roads should be increased by a factor of 4.76. Thus, the average erosion rate from roads on the jammer unit for 1.35 years preceding logging was 56.2 tons/sq. mile/day, and the average rate for 4.8 years following logging was 51.0 tons/sq. mile/day.

The best way to appreciate the effects of road construction and logging on sediment movement is to compare the rates of sedimentation generated by these uses to rates for undisturbed lands. As mentioned earlier, landslides do occur on undisturbed lands in the vicinity of the study area. However, data for erosion plots and sediment dams do not include any of these natural landslide events. Fortunately, sediment data collected in the same manner as used in this study are available from other similar watersheds in the immediate vicinity. These other watersheds are the Oompaul, Hamilton, Tailholt, and Circle End drainages of 740, 460, 1,625, and 930 acres in size, respectively. Sediment data were collected on one or more of these watersheds during the six-year study period and these data include the effects of natural landslides within the drainages. The average sedimentation rate for the study period on the undisturbed watersheds (weighted for drainage area) was 0.07 tons/sq. mile/day.

Comparing impacts to this common base, we find that both of the skidding methods as applied in this study increased sediment production an average of about 0.6 times. This is in contrast to sediment production from erosion on jammer roads where increases averaged 800 times and 730 times for the first 1.35 year and subsequent 4.8 year post-construction periods, respectively. The average increase for the entire 6.15-year period following road construction was about 750 times the undisturbed erosion rate.

Conclusions

Erosion plot data collected over a period of more than five years indicated that there was no difference between erosion on the jammer and skyline logging units. The topography and road access on the skyline unit were not particularly suited for skyline logging so that the potential advantages of skyline skidding were not fully utilized. Downhill skyline skidding increased sediment deposition an average of 0.6 times that of similar undisturbed watersheds in the area. Based on the results of the erosion plot studies, it was concluded that jammer skidding would lead to a similar increase in sediment deposition.

In contrast, erosion from roads increased sediment deposition by an average of 750 times for the period of



Fig. 4. Mass erosion on a jammer road in the Deep Creek study area due to poor road location and construction practices.

over six years following construction. The roads in question are typical of secondary logging roads on steep slopes in the area. Certainly erosion will vary considerably depending on many factors; however, it is felt that this study presents an accurate picture of the order of magnitude of impact to be expected from road construction in small drainages under similar conditions.

Jammer logging in the past has required a dense network of roads with a maximum road spacing of about 400 ft. In steep country this may disturb soil on 25 percent of the total logging area. Skyline logging systems permit road spacing up to 1,600 ft. or more, depending on the local conditions. This reduces the area disturbed by perhaps 75 percent and may provide a greater buffer area for sediment deposition between the roads and the stream channel. Thus, by far the greatest benefit to be derived from skyline logging systems with respect to erosion reduction results from reduced road mileage. This benefit lends impetus to logging systems that require even fewer roads than skyline systems on highly unstable lands. As an example, balloon logging is presently being conducted in the steep mountains in central Idaho.

The impact of road erosion indicates the obvious need for proper location, construction, and stabilization of logging roads and the use of good maintenance practices. Such practices have been shown to be feasible on roads constructed in the vicinity of the present

study. Gardner *et al.*³ indicate that much of the mass erosion can be eliminated by proper road location and construction. Bethlahmy and Kidd (2) found that sediment production resulting from surface erosion on fill slopes could be reduced more than 95 percent by application of grass seed and fertilizer protected by a straw mulch and wire netting.

Jammer logging systems on steep mountain lands are unacceptable in many areas due to excessive sediment production. Skyline logging greatly alleviates this hazard, but even this system is unacceptable in areas of extreme erosion hazard when roads are not properly constructed.⁴ The alternatives are: (a) ignore the damages that result; (b) eliminate logging; (c) develop logging systems that require fewer roads and accept the responsibility and cost of properly locating, constructing and maintaining roads.

³ Gardner *et al.* See footnote 2.

⁴ F. Jensen and L. Finn. Hydrologic analysis of the Zena Creek logging study area. Unpub. rep., Payette National Forest, McCall, Idaho. 123 p. 1966.

Literature Cited

1. BANCROFT, T. A., and R. L. ANDERSON. 1952. Statistical theory in research. McGraw-Hill Book Co., Inc., New York.
2. BETHLAHMY, N., and W. J. KIDD. 1965. Controlling soil movement from steep road fills. U.S. Forest Serv. Res. Note INT-45, 4 p.
3. CRADDOCK, GEORGE W. 1967. Zena Creek logging study evaluation report. USDA Forest Serv. Intermountain Region, Ogden, Utah, 63 p.
4. HAUPT, HAROLD F., and W. J. KIDD, JR. 1965. Good logging practices reduce sedimentation in central Idaho. *J. Forestry* 63:664-670.
5. RICHARDS, MONTE. 1963. Management of the chinook salmon fishery of the South Fork, Salmon River drainage. *Idaho Wildlife Rev.* 16(1): 3-7.

Sediment production from forest roads in western Oregon

Charles H. Luce and Thomas A. Black

USDA Forest Service, Rocky Mountain Research Station, Boise, Idaho

Abstract. Prevention and estimation of soil erosion from forest roads requires an understanding of how road design and maintenance affect sediment production. Seventy-four plots were installed on forest roads in the Oregon Coast Range to examine the relationship between sediment production and road attributes such as distance between culverts, road slope, soil texture, and cutslope height. An additional comparison was made between road segments with cutslopes and ditches freshly cleared of vegetation and segments with established vegetation on cutslopes and in ditches. All road segments were 5 m wide and insloped with aggregate surfacing, light traffic, and no overhanging forest cover. Sediment production was correlated to the product of segment length times road slope squared. Sediment production from aggregate covered roads on a silty clay loam was about 9 times greater than that from roads constructed on a gravelly loam. Sediment production was not correlated to the cutslope height. Road segments where vegetation was cleared from the cutslope and ditch produced about 7 times as much sediment as road segments where vegetation was retained, showing the potential reduction in erosion by revegetation following construction and the potential impact of ditch cleaning during maintenance. Relationships and estimates from this study provide a basis for improved erosion estimates by commonly used empirical procedures.

1. Introduction

Assessment of road contributions to sediment budgets generally relies on a summation of sediment production of each road segment multiplied by the fraction delivered to the stream [Cline *et al.*, 1984; U.S. Department of Agriculture (USDA) Forest Service Northern Region, 1991; Washington Forest Practices Board, 1995; Dubé *et al.*, 1998]. Predictions of the sediment production from road segments in these models are based on empirical observations [e.g., Megahan and Kidd, 1972; Megahan, 1974; Reid and Dunne, 1984; Bilby *et al.*, 1989; Swift, 1984], extension of rainfall simulation results [e.g., Burroughs and King, 1989; Burroughs *et al.*, 1992], and professional judgment. Recently, physically based modeling has been proposed as an alternative [Elliot *et al.*, 1995; Tysdal *et al.*, 1997]. The accumulated empirical evidence provides insight on how sediment yield is affected by traffic [Reid and Dunne, 1984; Bilby *et al.*, 1989; Foltz, 1999], surfacing [Foltz, 1999; Foltz and Elliot, 1997], and time following construction [Megahan, 1974]. There are a few limited observations on the effects of road slope [e.g., Vincent, 1985; MacDonald *et al.*, 1997] and cutslope height [e.g., U.S. Department of Agriculture (USDA) Forest Service Intermountain Forest and Range Experiment Station, 1981; Boise State University Department of Geology and Geophysics, 1984] on road sediment production. Data on the influence of road segment length, soil texture within a given climate, and maintenance practices on road segment sediment production are likewise limited or missing. These are important attributes of forest roads, and observations are needed to describe these effects in empirical models and verify predictions of physically based models. Here we describe how the sediment yield of a forest road segment (tread, cutslope, and ditch output through

This paper is not subject to U.S. copyright. Published in 1999 by the American Geophysical Union.

Paper number 1999WR900135.

a culvert or crossdrain) relates to road segment length, road slope, cutslope height, soil texture, and maintenance practices.

2. Theory

Erosion is the result of the interplay between the ability of flowing water to remove sediment, transport capacity, and the availability of moveable sediment. There are two aspects to the concept of availability as applied to forest roads, material erodibility, and loose soil supply. The material with which road treads are built is generally well compacted during construction, reducing its erodibility. Road construction and maintenance practices, however, disturb a layer of soil on the road tread, ditch, and cutslope that is the source of the most easily eroded material [Megahan, 1974]. Both the erodibility and the supply of this “loose” material play a role in the sediment yield from a road segment. Using these concepts, we will develop specific hypotheses regarding the relationship of sediment yield to road segment length, slope, cutslope height, soil texture, and maintenance.

2.1. Length and Slope

Mass conservation dictates that

$$E = \nabla \cdot Q_s \quad (1)$$

where E is the change in storage of soil in an area (erosion) and Q_s is the sediment transport rate. For a small volume above a small area on the ground (infinitesimally small in both cases), the amount of sediment leaving the volume is the same as the amount flowing into the volume plus any erosion that occurs over the small area. For a small watershed, such as the cutslope, tread, and ditch of a road, (1) may be evaluated as

$$E = Q_{s(\text{out})} \quad (2)$$

The basin's sediment discharge, $Q_{s(\text{out})}$, depends on the transport capacity and incoming sediment to the exit point. To

calculate the incoming sediment flux requires integrating detachment along the slope. Detachment at any point along the slope is not necessarily related to transport capacity. *Foster and Meyer* [1972, 1975] and *Lei et al.* [1998] describe methods to account for the difference between transport capacity and actual sediment flux. In general, however, on long plots with easily detached noncohesive materials (such as a ditch immediately following a grading operation), transport capacity at the end of a hillslope and the actual sediment discharge can be nearly equal [*Kirkby*, 1980; *Nearing et al.*, 1997]. Consequently, immediately following disturbance, we expect sediment production to be closely related to transport capacity.

Sediment transport capacity can be defined by one of two models:

$$Q_s = k(\tau - \tau_c)^{n_\tau} \quad (3)$$

$$Q_s = k(\Omega - \Omega_c)^{n_\Omega} \quad (4)$$

where k is some index of mobility of the sediment, τ is shear stress, τ_c is the critical shear stress for incipient motion, n_τ is an exponent between 1 and 2 [*Foster and Meyer*, 1975; *Kirkby*, 1980], Ω is the stream power, Ω_c is the critical stream power for incipient motion, and n_Ω is an exponent between 1 and 1.5 [*Govers*, 1992; *Bagnold*, 1977]. Shear stress, τ , is given by

$$\tau = \rho_w g d S \quad (5)$$

where ρ_w is the density of water, g is gravity, d is the depth of flow (alternatively hydraulic radius), and S is the water surface slope, usually accepted to be the same as the bed slope. Stream power, Ω , is given by

$$\Omega = \rho_w g q S \quad (6)$$

where q is the flow per unit width. Bringing in a simple relationship for the hydrology of a particular event, considering a nearly impermeable forest road [*Luce and Cundy*, 1994] at steady state flow,

$$q \propto x \quad (7)$$

where x is distance downslope, and that depth is a square root function of flow [*Dunne and Dietrich*, 1980]

$$d \propto \sqrt{q} \quad (8)$$

that yields two approximations for sediment transport at the end of the ditch. By the argument stated earlier regarding the close relationship between transport capacity and sediment flux, road segment sediment production from a segment of length, L is

$$E \propto k(S\sqrt{L} - \tau_c)^{n_\tau} \quad (9)$$

$$E \propto k(SL - \Omega_c)^{n_\Omega} \quad (10)$$

In the model based on shear stress transport, erosion is proportional to the product of slope and the square root of length with an exponent slightly greater than 1. In the model based on stream power, it is proportional to the product of length and slope with an exponent slightly greater than 1. Both equations suggest a statistical interaction effect for length and slope. Because plots with higher slopes exceed the critical shear stress for a greater fraction of the plot, transport capacity may be more fully sated at the bottom of steeper plots yielding a slightly stronger effect on slope, S , than predicted solely from the transport capacity. For this reason, we also considered an

increase in the exponent of slope relative to the exponent for length. The general form of an interaction between length and slope is supported by empirical erosion models developed on agricultural plots such as the Universal Soil Loss Equation (USLE) and the Revised Universal Loss Equation (RUSLE) [*Wischmeier and Smith*, 1978; *McCool et al.*, 1987, 1989; *Renard et al.*, 1994].

On the basis of the above discussion and the cited empirical observations, we hypothesize that sediment yield from road segments is related to plot length and slope according to a linear combination of L or \sqrt{L} , S or S^2 , and one of the four interaction terms (LS , LS^2 , \sqrt{LS} , and $\sqrt{LS^2}$). Arguments for why sediment yield should vary with L , \sqrt{L} , and S and their interactions are clear from (9) and (10). We also considered the increased role that slope might play in satisfying transport capacity at the end of the plot and the fact that n_τ can vary between 1 and 2 by considering a nonlinear slope term.

2.2. Cutslope Height

The effects of cutslope height on sediment production must be considered in light of the roles of transport capacity and loose sediment supply. Conceptually, flow and transport in the ditch control the sediment yield of an insloped road segment. Flow comes into the ditch from the road surface and the lower parts of the cutslope. The cutslope also contributes loose material to the ditch through a variety of processes, including soil creep, sheet wash, rilling, raveling, and slumping. Higher cutslopes produce more material [*USDA Forest Service Intermountain Forest and Range Experiment Station*, 1981; *Boise State University Department of Geology and Geophysics*, 1984]. If the initial loose sediment supply in the ditch is limiting, sediment yield over the course of a season should be higher on road segments with high cutslopes.

2.3. Soil Texture

Depths of flow and turbulence are not so great from a 100 m long road segment that all soil particles travel as suspended load. Larger particles move more slowly than smaller particles in saltating transport. *Burroughs et al.* [1992] describe soil erodibility as a function of soil texture and found that erodibility (for 0.6 m² plots under a rainfall simulator) was low in soils with high clay content (due to particle aggregation) and in soils with high sand content. The erodibility of soils with a high silt fraction was the greatest. Because the ditch is commonly set in the native soil, we expect that road segment sediment production will be greater on silty soils than on sandy soils.

2.4. Maintenance

Ditch maintenance removes vegetation that holds sediment in place and breaks up any armoring that may have occurred earlier. Effectively, this practice increases the supply of easy-to-transport loose sediment supply. The expectation is that ditch cleaning will increase sediment yields. Road grading should also increase yields but less dramatically because ditch vegetation is retained and aggregate surfacing is less erodible than the native soils in the ditches.

3. Methods

The general approach used to examine these questions and hypotheses was statistical inference based on sampling of sediment production from road segments. Sediment production was measured using sediment traps.

The study was conducted west of Eugene, Oregon, in the Oregon Coast Range (Figure 1). The central Oregon Coast Range receives between 1800 and 3000 mm of rainfall annually, with drier portions being further inland and wetter portions near the crest [Miller *et al.*, 1973]. Winters are mild and wet; summers are warm and dry. Plots are located between 250 and 600 m in elevation, below elevations where snow commonly accumulates. Soils are derived from sedimentary and metasedimentary rocks through most of the Coast Range with some igneous dikes in the inland foothills. The Tyee arkosic sandstone formation is the dominant bedrock throughout this part of the Coast Range. Douglas-fir and Western Hemlock forests cover much of the Coast Range.

Two field areas were used to examine sediment production on two soil textures. Many of the plots were located near Low Pass, Oregon. These sites were on the finer textured soils of the inner Coast Range. Soil series at Low Pass were Jory and Belpine silty clay loams. The Jory soil is a clayey, mixed, active, mesic Palehumult; the Belpine soil is a clayey, mixed, mesic Xeric Haplohumult. The other plots were located near Windy Peak, 15 km west of Low Pass and had coarser soils. The soils at Windy Peak were the Bohannon gravelly loam, a fine loamy,

Table 1. Factors Considered in the Study Design and How They Were Treated

Variable	Treatment
Soil Type	two soils selected: silty clay loam and gravelly loam
Segment length	three levels used: 40, 60, and 110 m
Road slope	varied from 3 to 12%
Cut-slope height	varied from 0.5 to 4 m
Time since construction	0 years and 15 years
Degree of rutting	all plots bladed at beginning
Inslope/crown/outslope	all plots bladed to inslope at beginning
Aspect	not controlled
Cut-slope slope	not controlled: higher cutslopes tend to be steeper
Slope position	all in upper third of hillslope
Road width	all roughly 5 m
Rainfall	differs between soils; recorded at both sites after 1st year
Forest cover	all plots in clearcut areas
Surfacing	basalt aggregate existing at all sites
Road use	all have light recreational and administrative traffic

mixed, mesic Andic Haplumbrept, and the Digger gravelly loam, a loamy-skeletal, mixed, mesic Dystric Eutrochrept.

3.1. Study Design

Major factors affecting sediment production from a forest road are (1) inherent erodibility and runoff producing capacity of the soil and running surface, (2) road segment length, (3) road gradient, (4) amount of cutslope and running surface, typically a function of road width and side slope, (5) treatments of cutslope, running surface, and fillslope, such as surfacing, straw, or jute mat, (6) flowpath geometry as embodied in insloping and outsloping and degree of rut development, (7) slope position and aspect in so far as they affect soil moisture, (8) forest cover, (9) time since construction, (10) road use, and (11) weather at the site, as indexed by rainfall erosivity. This study was designed to evaluate only a few of these factors. We attempted to control the other factors. Table 1 lists the variables embodied by these 11 factors and how each was treated in the study.

Three experiments were conducted. The first experiment was set up to examine the effects of road segment length and road slope or gradient. The second experiment was directed toward the effect of cutslope height on different soils. The third experiment focused on the effect of vegetation removal from the cutslope and ditch.

The study examining the effects of road segment length and road slope was carried out at the Low Pass site. Segment length was divided into three general classes: short (~40 m), medium (~60 m), and long (~110 m). Road slope was also divided into three general classes: low (4–6%), medium (6–11%), and steep (11–13%). Road length and slope were varied so that there were two replications in each of the nine combinations of length and slope, yielding 18 plots. This arrangement was used to assure that multicollinearity did not prevent examination of the interaction term between length and slope during regression analysis. Plots in the length-slope experiment were selected with cutslope heights in the medium category (2–4 m). Roads were freshly bladed, and cutslopes and ditches were cleared of vegetation.

The cutslope height experiment was carried out at both sites to introduce variability due to soils. Plots in the cutslope height

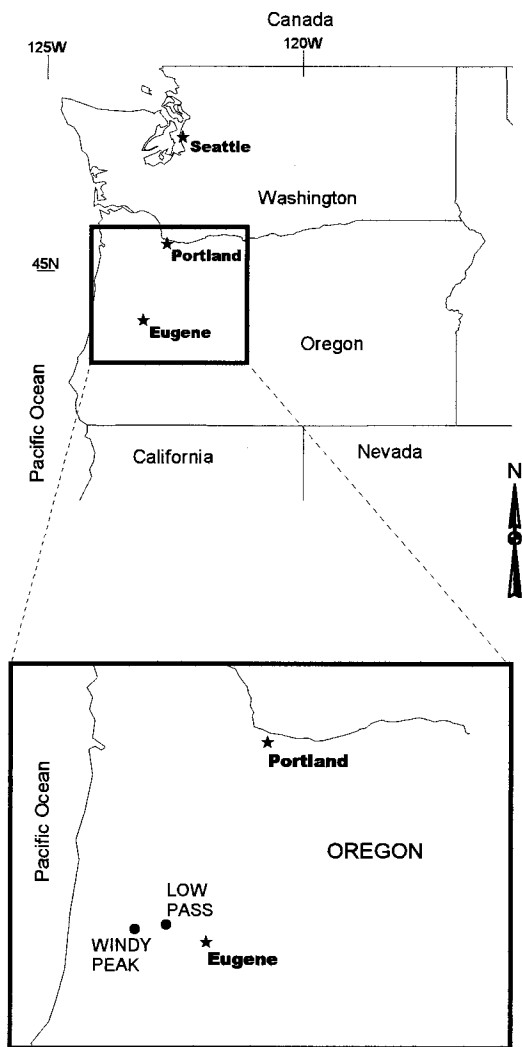


Figure 1. Location map with inset of northwestern Oregon showing the location of the two study areas, Low Pass and Windy Peak.

experiment had cutslope heights in three classes determined by the slope length of the cutslope: low (0–2 m), medium (2–4 m), and high (>4 m). These classes were used for plot selection to ensure that a comparable range and set of cut slopes were used at each study area. Two replications of each class for each soil yielded an additional 12 plots. This design allowed an analysis of covariance with the continuous cutslope height variable and the categorical soil variable. All cutslope height plots had medium lengths and medium slopes. Roads were freshly bladed, and cut slopes and ditches were cleared of vegetation.

The ditch and cutslope clearing experiment was also conducted at Low Pass. Three classifications of road treatment were considered for this experiment: no treatment, road tread graded, and road tread graded with cleared ditch and cutslope. The five plots with no treatment were installed 1 year earlier and had a range of slopes, and lengths, all with medium cutslope heights. Plots with the road treatment only were selected to have a matching set of plots. The five plots with road grading and cleared ditches and cut slopes were selected from among the length slope experiment plots to match the lengths and slopes of the five no-treatment plots.

In addition to the 40 plots required for these experiments, 34 more plots were installed in the area for replacement plots (in case of failure or vandalism) and for the later examination of temporal trends. Vandalism was widespread and regular but consisted mostly of shot sediment traps that were easily repaired. Ditch dams used to hydrologically isolate individual road segments were breached upslope of five plots during a large precipitation event. Those data were removed from examination.

General road characteristics common to the plots are 5 m width, basalt aggregate surfacing, insloped with ditch and crossdrains, recreational and administrative (light) traffic, and no forest cover. Aggregate for most of the roads came from two basalt quarries. Nelson Mountain quarry had a coarse durability of 78, a fine durability of 48, LA abrasion of 21%, and sulfate soundness of 7% loss [American Association of State Highway and Transportation Officials, 1995]. Conser quarry igneous intrusives had a coarse durability of 66, a fine durability of 76, and an LA abrasion of 19%.

The degree of rutting in the road has been cited as an important factor in sediment production of the road surface [Foltz and Burroughs, 1990]. Initial rutting was removed on all but five plots by grading the roads. The relatively equal surfacing and levels of traffic are expected to yield similar levels of rutting on the graded plots over time. All roads were insloped with water bars and crossdrains to make the contributing area for each sediment trap constant over time. With an insloped road and waterbars, all runoff and sediment generated on the road surface eventually reached the ditch.

Megahan [1974] demonstrated that time since construction is an important determinant in road erosion. In this study, we used roads that have been in place between 10 and 25 years. For the cutslope height and length-slope experiments, we bladed the road surface and scraped all vegetation from the cut slopes to simulate the effects of new road construction. At the time that the data presented in this paper were collected, the plots had been in operation for 1 year. Three more years of study are planned to measure the variation in sediment production over time. Five plots at the Low Pass site were left in the original, ungraded, vegetated condition for comparison to the experimentally treated plots.

The steepness of the cutslope may affect how much sedi-

ment is produced by a cutslope. In general, the cutslope gradient is designed when the road is engineered and constructed and depends on soil properties. It is also, in practice, a function of cutslope height. Low cut slopes are built in weaker surface soils and therefore have shallower gradients. Higher cut slopes intersect lower soil horizons and sometimes bedrock. Typical low cut slopes had gradients of 3:1, and medium cut slopes were around 2:1 on both soils. Higher cut slopes were between 2:1 and 1:1, generally steeper at the Windy Peak sites.

As constructed, forest roads do not have neatly defined segments with relatively constant slopes or cutslope heights. We installed waterbars and crossdrains (Figure 2) to hydrologically isolate relatively homogeneous road segments with the characteristics we wished to investigate. Cement inlet structures were placed to collect flow from the ditches, and runoff was routed under the road through 15.24 cm (6 inch) plastic pipe crossdrains to the sediment traps. Only sediment carried through this crossdrain was measured. The results of Megahan and Ketcheson [1996] showed that most sediment from roads and the sediment that is carried the farthest downslope is carried through crossdrains.

3.2. Sediment Traps

Sediment traps were 1.5 m³ plastic bins placed below the outlets of the crossdrains. Tanks were weighed with four load cells on jacks; the water was level across the top of the tank with the tank overflowing. These tanks have since been replaced by steel tanks of similar dimension (Figure 3) that can be weighed with a crane. The mass of the tank was measured with sediment and water and with water only. The mass of sediment was calculated from

$$M_s = (M_{ts} - M_{tw})\rho_s / (\rho_s - \rho_w) \quad (11)$$

where M_s is the mass of sediment, M_{ts} is the mass of the tank, sediment, and water, M_{tw} is the mass of the tank with water only, ρ_s is the particle density of the sediment, and ρ_w is the density of water (1000 kg/m³). Here ρ_s was estimated to be $2.65\rho_w$ (2650 kg/m³).

The attributes of several types of sediment traps were explored by Ice [1986]. This type of trap had the best trap efficiency of the several Ice explored. Foltz [1999] used a much smaller sediment trap for shorter road segments and estimated efficiencies for silt and finer fractions to be 40–60%. The few measurements of trap efficiency that we have taken indicate that an overflowing tank with 1/3 of its volume filled with sediment captures 70–80% of the fraction finer than silt (50 μ m) and all of the larger fractions during a 12 mm/hr storm. At Low Pass, where the soil is finer, an average of 8% of the soil fraction finer than 2 mm was finer than 0.05 mm based on aggregate particle size analysis as described by Kemper and Rosenau [1986]. Three traps filled with sediment during the largest event of the measuring period. Fortunately, the overflow from two of the traps deposited on large flat benches below the traps and the bypassed volumes were estimated from those deposits.

3.3. Climate Measurements

Climate observations were made in an open area at the Low Pass site. Precipitation was measured with a 0.254 mm/tip tipping bucket gage with 152.4 mm orifice. Temperature, relative humidity, wind speed, and direction were also measured.

The Low Pass site is 15 km farther inland and is 300 m lower

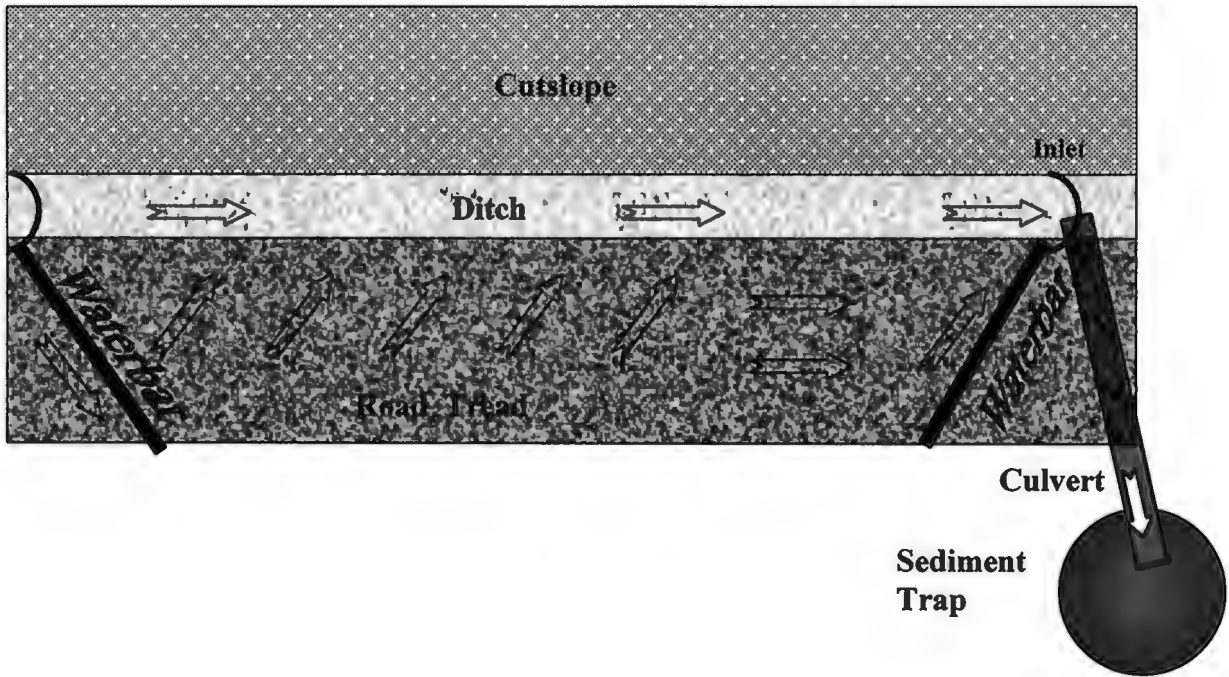


Figure 2. Typical plot layout.

in elevation than the Windy Peak site, so it almost certainly receives less precipitation. This difference is implicit in any comparisons between soils. All plots on a particular soil are within 2 km of each other.

For the period of study, November 1995 to February 1996, 1017 mm of rain fell at Low Pass. While the entire period was wetter than normal, the storm of February 6–7, 1996, was responsible for the greatest amount of runoff and sediment production. Peak hourly rainfall intensities for this storm were in the range of 10 mm/hr (Figure 4).

3.4. Statistical Analyses

Road segment length and slope data were analyzed by linear regression. Sediment yield data were regressed against multiple combinations of the variables listed in the theory section (L , \sqrt{L} , S , S^2 , and their interaction terms) to determine the best linear combination of these variables using fit, significance, and parsimony as criteria. For the better fitting models where the intercept was not significant, the prediction sum of squares (PRESS) statistic was used as a criterion. The PRESS



Figure 3. Photograph of sediment trap with crossdrain outlet.

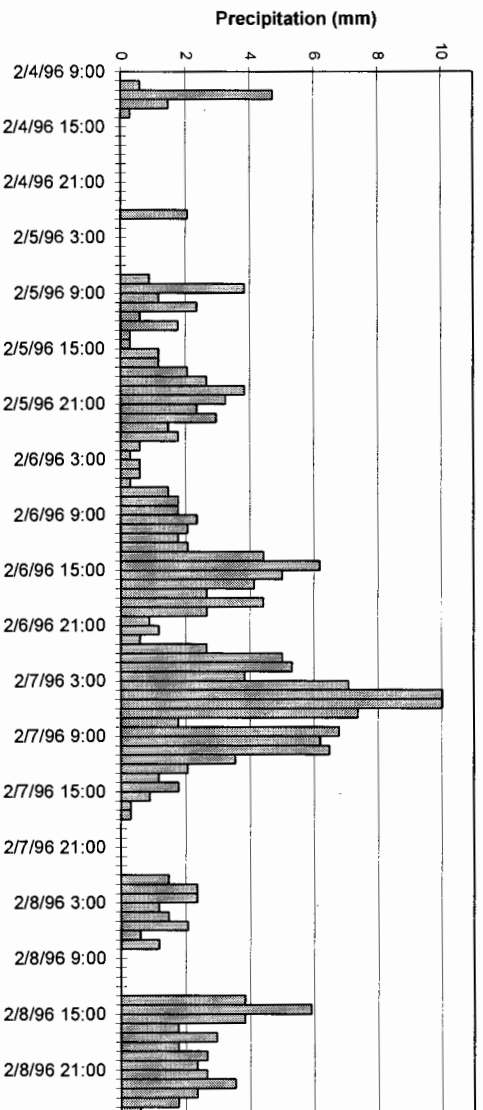


Figure 4. Hourly hyetograph for early February 1996, when the largest runoff event of the study period occurred.

statistic is calculated through a cross-validation procedure where the error for a point is found from the difference between the point and a line regressed through all of the other points. These are prediction errors of the model, which are summed and squared to yield PRESS. Normalizing the PRESS statistic by the variance times $(n - 1)$ yields the R_{pred} statistic, which gives an impression of how well the model can be used for prediction. Because plot length was a regression variable, we did not normalize by length to estimate per-unit-length or per-unit-area sediment production. Part of the purpose of the regression study on length was to determine whether unit area scaling is appropriate for road erosion.

Analysis of covariance was used to analyze the difference in sediment production between soils given the variation in cutslope height among plots, and separate regressions were done for each soil to estimate the effect of cutslope height on sediment production. Analysis of variance was used to compare the three maintenance treatments.

4. Results and Discussion

From November 1995 to February 1996, varying amounts of sediment were collected in the 68 surviving sediment traps (Figure 5). The most striking feature of these observations is the large range of sediment masses collected. In general, most road segments produced little sediment, but a few produced a large amount. This shows that substantial amounts of sediment can come from relatively standard roads with little use and that it may be possible to substantially reduce road erosion by targeting those few sections with the greatest sediment production. Given the wide range of characteristics for these roads, it is important to understand the sources of variability.

4.1. Relationship of Sediment Production to Segment Length and Slope

Figure 6a shows the relationship of sediment production to segment length by slope class, and Figure 6b shows the relationship of sediment production to slope by segment length class. The figures show that increases in both road length and gradient can lead to increased erosion. The interaction between length and gradient is strong in both figures. For example, increasing length has little effect if the gradient is low but

has a great deal of effect on roads with high gradients. The difference in how sediment production relates to gradient for different length classes in Figure 6b seems mostly to be change in slope of the graphs as opposed to a shift in position. This indicates that the interaction term in a regression would be potentially more important than either length or road slope alone.

The r^2 , adjusted r^2 (includes a penalty for increased number of parameters), and p value (indicates significance of relationship) for several combinations of length, slope, and interaction terms are reported in Table 2. The best models, given the criteria of fit and parsimony, appeared to be those that included only one of the four interaction terms. For each of these, the intercept was not statistically different from zero, and because we believe that for zero length or slope the erosion would be nominally zero, regressions with the intercept set to zero were tested. Table 3 shows a comparison of the four interaction-only models with zero intercept using the prediction sum of squares (PRESS). On the basis of this analysis, the model

$$E = 717 LS^2 \quad (12)$$

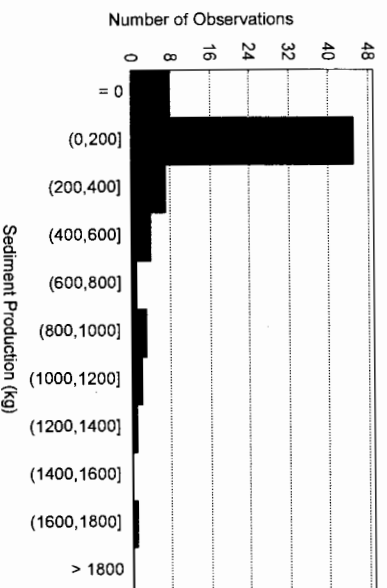


Figure 5. Histogram of sediment production from all plots. The range (x -axis) and relative frequency (y -axis) of sediment produced during the study period from a large variety of road plots are shown.

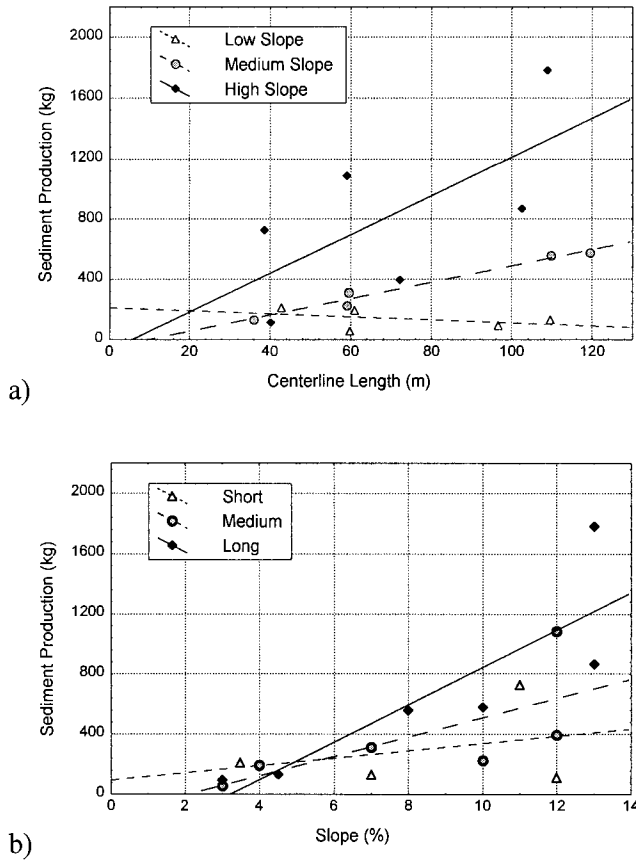


Figure 6. Sediment production as a function of (a) segment length lumped by three slope classes and (b) road slope lumped by three length classes.

had the best predictive ability. Erosion is plotted against LS^2 in Figure 7.

Embodied within the constant obtained from this regression is information on soil erodibility, the runoff producing capability of the road and ditch, the rainfall erosivity experienced in this period of time, and the antecedent moisture conditions for a given rainfall event. This constant may well be meaningless

Table 3. R_{pred} Scores for the Four Zero-Intercept Models

Model	R_{pred}	SE_{est}	F	p
$E = aLS$	0.43	302.75	58.2	0.000001
$E = aLS^2$	0.51	273.92	74.41	<0.000001
$E = aL^{1/2}S$	0.42	310.36	54.65	0.000002
$E = aL^{1/2}S^2$	0.49	282.22	69.23	0.000001

outside of this context, and the more useful relationship is the general

$$E \propto LS^2 \tag{13}$$

On the basis of this relationship, measurements from a road with known slope and length for a soil and climate of interest can be extrapolated to apply to roads with differing slopes and lengths but otherwise similar characteristics. The exponent for slope agrees well with observations by Vincent [1985] and McCool *et al.* [1987], who found nonlinear, concave-upward, relationships between slope and erosion. The exponent for L disagrees with the square-root relationship identified by Wischmeier and Smith [1978], although the difference in fit is small (Table 3). McCool *et al.* [1989] suggested that the exponent should be closer to one for situations where rill erosion dominates over rainsplash in delivery of sediment. Given the uncertainty in the literature about exponents for (9) and (10) and the similarity in fit for LS^2 and $\sqrt{LS^2}$, it is difficult to say whether the shear stress model or the stream power model is better supported by these data. However, the best fit to the data agrees well with the basic model form derived from consideration of either a shear stress or stream power conceptualization. This physical basis lends credence to this model form for use in other soils and climates.

4.2. Relationship of Sediment Production to Underlying Soil and Cutslope Height

Examination of data from the cutslope height and soil texture experiment shows a strong relationship with soil texture and a weak relationship with cutslope height (Figure 8). Average sediment production was 473 kg for the Low Pass plots and 51 kg at Windy Peak, a factor of 9.3 times greater. Analysis of covariance showed that this difference was statistically sig-

Table 2. Statistics of Selected Models Used to Fit the Length and Slope Versus Sediment Production Data

Model	R^2	Adjusted R^2	p
$E = aL + b$	0.131	0.068	1.7E-01
$E = aS + b$	0.452	0.413	4.3E-03
$E = aL^{1/2} + b$	0.126	0.064	1.8E-01
$E = aS^2 + b$	0.494	0.458	2.4E-03
$E = aLS + b$	0.580	0.550	6.1E-04
$E = aLS^2 + b$	0.658	0.638	1.4E-04
$E = aL^{1/2}S + b$	0.600	0.571	4.3E-04
$E = aL^{1/2}S^2 + b$	0.629	0.603	2.5E-04
$E = aL + bS + c$	0.543	0.473	6.1E-03
$E = aL + bS^2 + c$	0.577	0.512	3.6E-03
$E = aL + bLS^2 + c$	0.662	0.610	8.7E-04
$E = aS + bLS^2 + c$	0.658	0.605	9.0E-04
$E = aS^2 + bLS^2 + c$	0.659	0.606	9.0E-04
$E = aL + bS + cLS^2 + d$	0.671	0.589	3.1E-03
$E = aL + bS + cLS + dLS^2 + e$	0.676	0.558	9.0E-03
$E = aL^{1/2} + bL^{1/2}S + cL^{1/2}S^2 + d$ (USLE)	0.646	0.558	4.8E-03

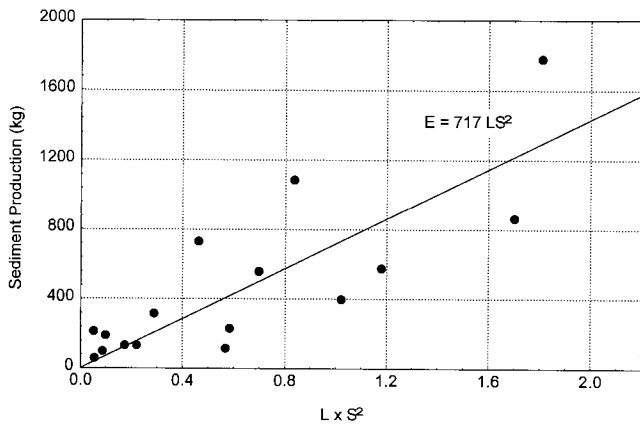


Figure 7. Erosion versus LS^2 . Note that 717 is a constant that would apply only for this study period and for these soils. The more general relationship is $E \propto LS^2$.

nificant [$p(M_{LP} = M_{WP}) = 0.002$]. This agrees with general theory in sediment transport and erosion that larger clasts and sediments are more difficult to move. Infiltration capacity may also be greater in the coarser soil. In general, Windy Peak would be expected to receive more rainfall than Low Pass because it is closer to the coast and has a higher elevation, emphasizing the role of soil in the difference between Low Pass and Windy Peak sediment production.

The slope of the relationship between cutslope height and sediment production at both sites is not significantly different from zero [$p(\beta_{LP} = 0) = 0.25$, $p(\beta_{WP} = 0) = 0.74$], although generally trending in the expected direction. From these data, cutslope height appears to have no effect on whole plot sediment production for freshly disturbed roads and ditches. On the basis of the concept of availability as discussed in the theory section, this finding suggests that loose sediment was available in all ditches throughout the study.

We observed abundant loose soil in the ditches at the be-

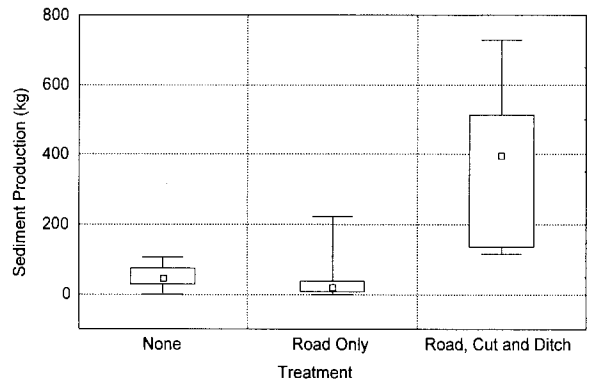


Figure 9. Sediment production versus road treatment for a subset of plots.

ginning of the season, so this is a reasonable possibility. High cutslopes may be a more important source of sediment in later years when sediment availability in the ditch of segments with stable noneroding cutslopes is reduced, implying that the time scale considered in this study is too short to show the effects of sediment depletion and vegetation regrowth in the ditch. This observation is supported by the results of the length and slope experiment.

4.3. Relationship of Sediment Production to Ditch and Cutslope Treatment

Cleaning ditches and removing the cutslope vegetation caused a dramatic increase in sediment production. Three groups of plots at Low Pass were used to measure the effect. The first group received no treatment and presents a 20 year old road with vegetated cutbank and ditch. The second group had only the road surface graded. The third group had the road graded, the ditch cleaned, and the cutslope stripped of vegetation. Figure 9 shows the range of values for each of the three treatments, with the mean sediment production at 50 kg for the untreated road, at 57 kg for the treated road tread, and at 377

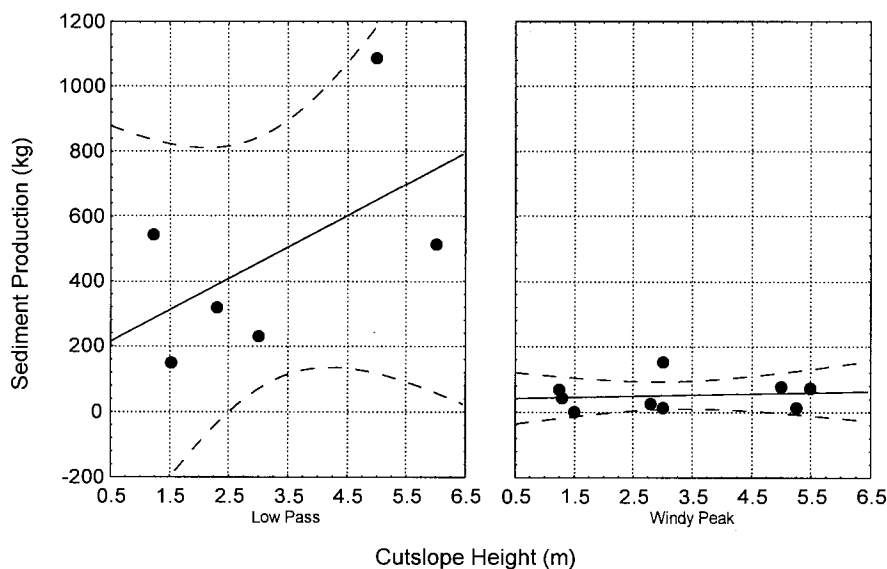


Figure 8. Sediment production versus cutslope height on each of the two soils. Soils at Low Pass are a silty clay loam, and soils at Windy Peak are a gravelly loam. The relationship between cutslope height and sediment production is not significant for either soil.

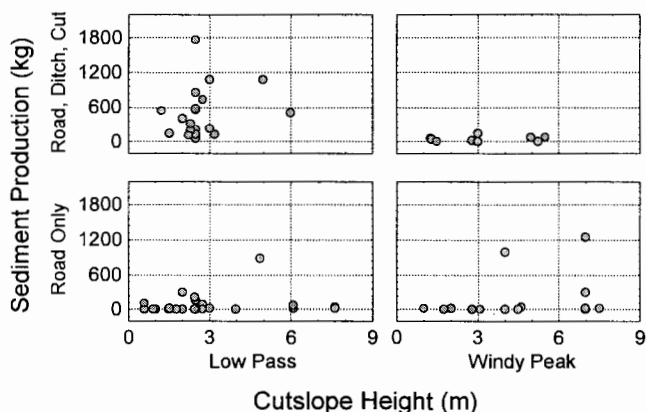


Figure 10. Sediment versus cutslope height for four different cases. The top graphs are for plots used in the experiments that were freshly bladed and with vegetation cleared on the cutslope and ditch. The bottom two graphs use “validation” plots that only received a treatment of the road surface. The data from the fine-grained soils at Low Pass from the coarser soils at Windy Peak are shown.

kg for the treated ditch and cutslope. Analysis of variance showed that the difference in sediment production among the three classifications was significant [$p(Mu = Mr = Mrc) = 0.0110$]. The difference between no treatment and roadway treatment was not significant [$p(Mu = Mr) = 0.95$], and the difference between either of those sets of plots and plots where the ditch and cutslope were treated was significant [$p(Mu = Mrc) = 0.008$, $p(Mr = Mrc) = 0.008$]. In these fine-grained soils, removing vegetation from the ditch and cutslope increased sediment production by a factor of 7.4 relative to no treatment and by a factor of 6.6 over treatment of the road surface only.

The question remains whether the differences in erosion are due to the cutslope contribution or the ditch contribution. Figure 10 shows four graphs of sediment production versus cutslope height. Two of the three anomalous points for plots with treated roadways only (the two lower plots) are cutslopes with unusual soil and bedrock conditions leading to a naturally bare cutslope and ditch, and the third anomalous point is a 250 m long 15% grade plot with a gullied ditch. None of the four scatterplots show any significant relationship between sediment production and cutslope height. At the same time there is a large difference between treated and untreated cut/ditch at Low Pass and a lesser but still noticeable difference at Windy Peak. From this, it can be concluded that the treatment of the ditch is probably a more important factor in the increased sediment production than the treatment of the cutslope, although, this may only be true for a short period following treatment of the ditch.

5. Summary and Conclusions

Sediment production by a forest road through surface erosion clearly depends on several factors. The data presented in this paper provide important insights into some of these dependencies. First, the variability in sediment production from road segment to road segment is high. Most segments produce little sediment, while only a few produce a great deal, implying that managing the sediment production of the few highest risk segments would be the most efficient. Second, sediment pro-

duction is proportional to the product of road segment length and the square of the slope (LS^2). The nonlinearity in the effect of slope is important to consider and demonstrates that road slope is an important attribute to consider in the assessment of sediment budgets. The use of a linear scaling of sediment yield by length (e.g., tons/mile) is supported by this relationship for road segments with lengths on the scale of tenths of kilometers. Third, soil texture has a strong effect on sediment yield, with coarser soils producing much less sediment than finer soils. This is a key area of uncertainty in most road erosion assessments. It is clear that measurements that show the relative erodibility of soils in the context of the entire road prism should yield significant improvement of these assessments. Finally, sediment yields from older roads with undisturbed ditchlines are much smaller than sediment yields from newer roads or roads with disturbed ditchlines. Disturbance of the road surface alone through grading showed less effect.

The results of this study give insights that are valuable when considering two important questions remaining unanswered by this study; the effects of time and of traffic. It is clear that time in a nominal sense, old and new, is important. Answers to the questions of how rapidly the changes occur and through what mechanisms would be useful when seeking the integrated sediment yield over some time period. In addition, the role of traffic in forming ruts and disturbing the tread surface is effective in interaction with processes occurring in the ditch. Previous studies suggest that rut formation and disturbance to the tread increases tread erosion. This study suggests that it is also important to consider the degree to which the rutting captures water that would otherwise be ditchflow and whether the increased erosion due to tread disturbance results in an increase to the total erosion from a road segment with a recently disturbed ditch.

Acknowledgments. This study was cooperatively funded by the Oregon State Office of the U.S. Department of the Interior, Bureau of Land Management, the National Council of the Pulp and Paper Industry for Air and Stream Improvement, and the U.S. Department of Agriculture, Forest Service, Rocky Mountain Research Station. A study of this scope cannot be accomplished without help from many people and organizations. In particular, we would like to thank Barry Williams and Clif Fanning of the USDI BLM for their continuing assistance in carrying out this study, Walt Megahan of NCASI, and Jack King, Randy Foltz, Bill Elliot, and Jim Clayton of the Rocky Mountain Research Station for helpful scientific discussions and reviews. This paper has benefited substantially from reviews by Terry Cundy and David Montgomery.

References

American Association of State Highway and Transportation Officials, *Standard Specifications for Transportation Materials and Methods of Sampling and Testing*, Am. Assoc. of State Highway and Transp. Off., Washington, D.C., 1995.
 Bagnold, R. A., Bed load transport by natural rivers, *Water Resour. Res.*, 13(2), 303-312, 1977.
 Bilby, R. E., K. Sullivan, and S. H. Duncan, The generation and fate of road-surface sediment in forested watersheds in southwestern Washington, *For. Sci.*, 35(2), 453-468, 1989.
 Boise State University Department of Geology and Geophysics, Sediment yield from cut and fill slopes, Silver Creek Research Road, Boise National Forest, Idaho, *Project Completion Rep. INT-80-003-CA*, 97 pp., Boise State Univ., Boise, Idaho, 1984.
 Burroughs, E. R., Jr., and J. G. King, Reduction of soil erosion on forest roads, *General Tech. Rep. INT-264*, 21 pp., U.S. Dep. of Agric., For. Serv., Intermountain Res. Stn., Ogden, Utah, 1989.

- Burroughs, E. R., Jr., C. H. Luce, and F. Phillips, Estimating interrill erodibility of forest soils, *Trans. ASAE*, 35(5), 1489–1495, 1992.
- Cline, R., G. Cole, W. Megahan, R. Patten, and J. Potyondy, Guide for predicting sediment yield from forested watersheds, rep., U.S. For. Ser. Northern Reg. and Intermountain Reg., Missoula, Mont., and Ogden, Utah, 1984.
- Dubé, K. V., and W. L. Wold, SEDMOD: A GIS-based road erosion and delivery model (abstract), *Eos Trans. AGU*, 79(45), Fall Meet. Suppl., F352, 1998.
- Dunne, T., and W. E. Dietrich, Experimental investigation of Horton overland flow on tropical hillslopes, 2, Hydraulic characteristics and hillslope hydrographs, *Z. Geomorphol. Suppl.*, 33, 60–80, 1980.
- Elliot, W. J., R. B. Foltz, and C. H. Luce, Validation of water erosion prediction project (WEPP) model for low-volume forest roads, *Proceedings of the Sixth International Conference on Low-Volume Roads*, edited by Transportation Research Board, pp. 178–186, National Acad. Press, Washington, D.C., 1995.
- Foltz, R. B., Traffic and no-traffic on an aggregate surfaced road: Sediment production-differences, paper presented at Seminar on environmentally sound forest roads and wood transport, Food and Agric. Organ., Rome, Italy, 1999.
- Foltz, R. B., and E. R. Burroughs Jr., Sediment production from forest roads with wheel ruts, *Proceedings: Watershed Planning and Analysis in Action*, edited by R. E. Riggins et al., pp. 266–275, Am. Soc. of Civil Eng., New York, 1990.
- Foltz, R. B., and W. J. Elliot, The impact of lowered tire pressures on road erosion, *Trans. Res. Rec.*, 1589, 19–25, 1997.
- Foster, G. R., and L. D. Meyer, A closed form soil erosion equation for upland areas, in *Sedimentation, Symposium to Honor Professor H. A. Einstein*, edited by H. W. Shen, pp. 12.1–12.19, Colorado State Univ., Fort Collins, 1972.
- Foster, G. R., and L. D. Meyer, Mathematical simulation of upland erosion by fundamental erosion mechanics, in *Present and Perspective Technology for Predicting Sediment Yields and Sources—Proceedings of Sediment-Yield Workshop, Agric. Res. Serv. Rep. ARS-S-40*, pp. 190–206, U.S. Dep. of Agric. Sedimentation Lab., Oxford, Miss., 1975.
- Govers, G., Evaluation of transporting capacity formulae for overland flow, in *Overland Flow Hydraulics and Erosion Mechanics*, edited by A. J. Parsons and A. D. Abrahams, pp. 243–273, Chapman and Hall, New York, 1992.
- Ice, G. G., A study of the effectiveness of sediment traps for the collection of sediment from small forest plot studies, *Tech. Bull. 483*, 27 pp., Natl. Council of the Pulp and Pap. Ind. for Air and Stream Impr. (NCASI), New York, 1986.
- Kemper, W. D., and R. C. Rosenau, Aggregate stability and size distributions, in *Methods of Soil Analysis, Part 1, Physical and Mineralogical Methods*, 2nd ed., pp. 425–442, Am. Soc. of Agron., Soil Sci. Soc. of Am., Madison, Wis., 1986.
- Kirkby, M. J., Modelling water erosion processes, in *Soil Erosion*, edited by M. J. Kirkby and R. P. C. Morgan, pp. 183–216, John Wiley, New York, 1980.
- Lei, T., M. A. Nearing, K. Haghigi, and V. F. Bralts, Rill erosion and morphological evolution: A simulation model, *Water Resour. Res.*, 34(11), 3157–3168, 1998.
- Luce, C. H., and T. W. Cundy, Parameter identification for a runoff model for forest roads, *Water Resour. Res.*, 30(4), 1057–1069, 1994.
- MacDonald, L. H., D. M. Anderson, and W. E. Dietrich, Paradise threatened: Land use and erosion on St. John, US Virgin Islands, *Environ. Manage.*, 21(6), 851–863, 1997.
- McCool, D. K., L. C. Brown, G. R. Foster, C. K. Mutchler, and L. D. Meyer, Revised slope steepness factor for the Universal Soil Loss Equation, *Trans. ASAE*, 30(5), 1387–1396, 1987.
- McCool, D. K., G. R. Foster, C. K. Mutchler, and L. D. Meyer, Revised slope length factor for the Universal Soil Loss Equation, *Trans. ASAE*, 32(5), 1571–1576, 1989.
- Megahan, W. F., Erosion over time: A model, *Res. Pap. INT-156*, 14 pp., U.S. Dep. of Agric. For. Serv., Intermountain Res. Stn., Ogden, Utah, 1974.
- Megahan, W. F., and G. L. Ketcheson, Predicting downslope travel of granitic sediments for forest roads in Idaho, *Water Resour. Bull.*, 32(2), 371–382, 1996.
- Megahan, W. F., and W. J. Kidd, Effect of logging roads on sediment production rates in the Idaho Batholith, *For. Serv. Res. Pap. INT-123*, 14 pp., U.S. Dep. of Agric. For. Serv., Intermountain For. and Range Exp. Stn., Ogden, Utah, 1972.
- Miller, J. F., R. H. Frederick, and R. J. Tracey, Precipitation frequency atlas of the United States, *NOAA Atlas 2*, U.S. Dep. of Commer., Nat. Weather Serv., Silver Spring, Md., 1973.
- Nearing, M. A., L. D. Norton, D. A. Bulgakov, G. A. Larionov, L. T. West, and K. M. Dontsova, Hydraulics and erosion in eroding rills, *Water Resour. Res.*, 33(4), 865–876, 1997.
- Reid, L. M., and T. Dunne, Sediment production from forest road surfaces, *Water Resour. Res.*, 20(11), 1753–1761, 1984.
- Renard, K. G., J. M. Lafren, G. R. Foster, and D. K. McCool, The revised universal soil loss equation, in *Soil Erosion Research Methods*, edited by R. Lal, pp. 105–124, Soil and Water Conserv. Soc., Ankeny, Iowa, 1994.
- Swift, L. W., Jr., Gravel and grass surfacing reduces soil loss from mountain roads, *For. Sci.*, 30(3), 657–670, 1984.
- Tysdal, L., B. Elliot, C. Luce, and T. Black, Modeling insloping road erosion processes with the WEPP watershed model, presented at the 1997 ASAE Annual International Meeting, Minneapolis, Minn., August 10–14, 1997.
- U.S. Department of Agriculture (USDA) Forest Service Intermountain Forest and Range Experiment Station, Horse Creek Administrative-Research Project, interim report on research, 212 pp., Ogden, Utah, 1981.
- U.S. Department of Agriculture (USDA) Forest Service Northern Region, WATSED, 125 pp., U.S. Dep. of Agric. For. Serv., Reg. 1, Missoula, Mont., 1991.
- Vincent, K. R., Runoff and erosion from a logging road in response to snowmelt and rainfall, M.S. thesis, 60 pp., Univ. of Calif., Berkeley, 1985.
- Washington Forest Practices Board, Standard methodology for conducting watershed analysis, Version 3.0, November 1995, pp. B1–B52, Wash. State Dep. of Nat. Res., Olympia, Wash., 1995.
- Wischmeier, W. H., and D. D. Smith, Predicting rainfall erosion losses, in *Agriculture Handbook 537*, 58 pp., U.S. Dep. of Agric., Washington, D.C., 1978.

T. A. Black and C. H. Luce, USDA Forest Service, Rocky Mountain Research Station, 316 East Myrtle Street, Boise, ID 83702. (cluce@rmci.net)

(Received June 26, 1998; revised April 19, 1999; accepted April 20, 1999.)